

Isogeometric analysis of C^1/G^1 dual mortaring and its application for multi-patch Kirchhoff-Love shell

Di Miao

Advisor: Michael J. Borden

*Department of Civil and Environmental Engineering
Brigham Young University
368 CB, Provo, UT 84602, USA*

1. Introduction

Isogeometric analysis was introduced by Hughes et. al. [50] in 2005, as a novel discretization technology. Since then, it attracted considerable attentions from the academic world and is enjoying explosive growth. The idea behind isogeometric analysis is to use the same basis functions for the geometric modeling and computational analysis. While the main aim of isogeometric analysis is to eliminate the geometric approximation error, it has been observed that, compared to traditional C^0 finite element, higher regularity Non-uniform Rational B-splines (NURBS) provide higher efficiency per degree of freedom [5, 30, 31]. Meanwhile, high regularity basis functions allow us to solve higher order partial differential equations (PDEs), e.g. the biharmonic equation [67, 57, 54], the Kirchhoff-Love shell problem [59, 58, 60] and the Cahn-Hilliard equation [43, 18, 17].

However, the higher dimensional NURBS basis functions are obtained by a tensor product of one-dimensional NURBS basis functions, which imposes limitations on its feasibility for analysis. Considering a scenario that a refinement is applied to a region of interest, however, for the tensor-product domain, it also introduces control points far from that region, which dramatically increases the problem size.

The adaptive finite element technique try to automatically refine a mesh in an optimal fashion so that a desirable discretization error level is achieved

22 with the fewest degrees of freedom. Based on the solution from a coarse
23 mesh, a *posteriori* error estimator provides a guidance for deciding where
24 and how to refine a mesh. It can increase the convergence rate, particularly
25 when singularities are present. However, this promising technique can not
26 be applied directly to NURBS mesh, as it does not support local refinement.

27 Since high smoothness basis function can be used in Isogeometric analy-
28 sis, the numerical approximation of high order PDEs can be realized in the
29 framework of the standard Galerkin formulation. However, without intro-
30 ducing mesh degenerations, it is impossible to parameterize geometries with
31 sharp corner or kink by high continuity meshes.

32 2. Literature review

33 To circumvent the shortcomings discussed above, various methods have
34 been proposed. The purpose of this section is to provide an overview of the
35 popular methods that endow B-spline meshes with multi-patch coupling and
36 local refinement abilities.

37 2.1. Local refinable splines

38 In 1988, Forsey and Bartels [41] introduced the hierarchical B-spline re-
39 finement algorithm, which can restrict the influence of refinement to the lo-
40 cality. The algorithm is achieved by a re-representation process that replaces
41 each basis function by an equivalent linear combination of a set of basis func-
42 tions defined by nested knot vectors. However, due to the lack of a natural
43 control grid, the hierarchical B-spline has not been widely recognized in the
44 CAD society, and a few applications can be found in geometric design. Re-
45 cently, this technique has been extended to Isogeometric Analysis, by Vuong
46 *et al.* [89]. Owing to the construction strategy, the resulted hierarchical
47 basis function are linearly independent and retain the maximal regularity,
48 which renders the hierarchical B-spline a good candidate for analysis. The
49 numerical tests demonstrate that the use of the hierarchical B-spline lead to
50 a superior performance for problems with corner singularity. A subdivision-
51 based hierarchical B-spline was proposed by Bornemann *et al.* [19], to tackle
52 the intricate algorithms in the software implementation of hierarchical B-
53 splines. The subdivision scheme establishes algebraic relations between the
54 basis functions and their coefficients defined on different refinement level
55 of the mesh and greatly ease the implementation of hierarchical B-splines.
56 Consecutively, the truncated basis for hierarchical splines (THB-spline) was

57 introduced by Giannelli *et al.* [42]. THB-splines is created by eliminating
58 from the coarse hierarchical basis function the contribution corresponding to
59 the subset of finer basis functions. Besides all the nice properties of hierarchi-
60 cal B-splines, the THB-splines obtain smaller support and form a partition
61 of unity, which lead to sparser matrices and lower condition numbers.

62 However, all the above hierarchical B-splines are still under the tensor
63 product formulism, which restricts hierarchical B-splines to a global rectan-
64 gular parametric domain. In order to represent complex topologies, subdivi-
65 sion schemes are widespread in geometry processing and computer graphics.
66 Among the most popular subdivision schemes are the Catmull-Clark [24],
67 Doo-Sabin [32] and Loop's [65] scheme. For Isogeometric Analysis, Wei *et*
68 *al.* [90] introduced truncated hierarchical Catmull-Clark subdivision (THCCS)
69 that can handle extraordinary nodes involved in complex topologies. THCCS
70 inherits the surface continuity of Catmull-Clark subdivision, namely C^1 con-
71 tinuity at extraordinary points and C^2 continuity elsewhere. Loop subdivi-
72 sion surfaces provides similar regularity properties as THCCS and has been
73 applied to Isogeometric Analysis in [53, 72] to generate triangular meshes.
74 One of the limitations in the implementation of subdivision meshes is that
75 the basis function around the extraordinary point is composed of piecewise
76 polynomial functions with an infinite number of segments, which leads to
77 insufficient integration by Gauss quadrature rule. To deal with this issue,
78 various quadrature rules and adaptive strategies have been examined in [68]
79 for Poisson problem on the disk and in [52] for fourth order PDEs.

80 In 2003, Sederberg *et al.* [81] introduced T-splines, which allows the
81 existence of T-junctions in the control grid, so that lines of control points
82 need not traverse the entire control grid. Thus, local refinement can be
83 realized by introducing T-junctions around interested region. Since the con-
84 cept of T-splines is a generalization of NURBS technology, it can be used
85 to merge NURBS surfaces that have different knot-vectors at the intersec-
86 tion. Therefore, the T-splines are also suitable to address trimmed multi-
87 patch geometries. Due to the desirable features of T-splines, Bazilevs *et al.*
88 [4] explored this technology in Isogeometric Analysis, and numerical results
89 demonstrated its potential for solving structural and fluid problems. By
90 utilizing the Bézier extraction operator, a finite element data structure for
91 T-splines [80] was developed to ease the incorporation of T-splines into ex-
92 isting finite element codes. However, it has been proven [23] that the original
93 definition of T-splines is not sufficient to ensure the linear independence of
94 the basis functions. To circumvent this issue, analysis suitable T-splines [64]

95 was developed by applying an additional constraint that no two orthogonal
96 T-junction extensions are allowed to intersect. Subsequently, the mathematical
97 properties of analysis suitable T-splines were studied in [63, 93], and it
98 has been successfully applied to the boundary element method [79]. Mean-
99 while, an adaptive local h-refinement algorithm with T-splines and a local
100 refinement of analysis-suitable T-splines were introduced by Döfel *et al.* [38]
101 and Scott *et al.* [78], respectively. However, for both algorithm, the refined
102 mesh is not as local as one could hope and this problem might be severe in
103 3D.

104 *2.2. Multi-patch geometrically continuous functions*

105 One of the advantages of Isogeometric Analysis is that it provides basis
106 functions with high smoothness, *i.e.* for p -th order splines, they enjoy up
107 to C^{p-1} continuity within a single patch. Thus, it is possible to directly
108 discretize differential operators of order higher than 2. However, continuity
109 higher than C^0 for multi-patch discretization imposes significant difficulties.
110 The conception of geometric continuity is very important in CAD field [74] for
111 designing smooth multi-patch domain containing extraordinary vertices [73].
112 In the parametric space, the geometric continuity of order s (G^s continuity)
113 is a weaker continuity constraint as compared to C^s continuity, while it has
114 been proved by Giroisser and Peters [44] that G^s continuity in the parametric
115 space is equivalent to C^s continuity of the basis function after the parametric
116 mapping. Thus, the construction of C^s isogeometric functions over a C^0
117 parameterization can be interpreted as geometric continuity G^s of the graph
118 parameterization. Bercovier *et al.* [12] has shown that for multi Bézier
119 patches over an unstructured quadrilateral mesh, as long as the order of
120 polynomial is high enough, there always exists the minimal determining set
121 for a C^1 continuity construction. Moreover, the resulting basis functions do
122 not contain subdivisions around extraordinary vertices.

123 The case of G^1 continuous functions on bilinearly parametrized two-patch
124 B-spline domains was considered by Kapl *et al.* [57], where the C^1 basis
125 functions are constructed and analyzed by numerical tests. It is shown that
126 the space dimensionality heavily depends on the parameterization of two
127 bilinear patch, and optimal convergence is observed on biharmonic problem.
128 However, over-constrained C^1 isogeometric spaces that causes sub-optimal
129 convergence is also observed for certain configurations (*e.g.* two-patch non-
130 bilinear parameterizations and C^{p-1} continuity within the patches for p -th
131 order spline space). A theoretical analysis of the causing of C^1 locking is

132 provided in [26], where the analysis-suitable G^1 geometry parameterization,
133 that allows for optimal approximation of C^1 isogeometric spaces, is identified
134 and testified by numerical examples. The methods in [57] has been extended
135 to bilinearly parameterized multi-patch domains in [54], where the simple
136 explicit formulas for spline coefficients of C^1 basis function is derived and
137 nested C^1 isogeometric spaces are generated. Recently, Kapl *et al.* [56,
138 55] explored the construction of C^2 isogeometric functions on multi-patch
139 geometries and utilized the C^2 isogeometric spaces for 6-th order PDE.

140 Although the geometrically continuous functions circumvent the use of
141 subdivisions for domains with extraordinary vertices, the requirement of C^0
142 parameterization averts local mesh refinement, and lower continuity is re-
143 quired to avoid C^1 locking effect. Thus, its implementation can be complex
144 and it may not be a potential candidate for analysis in more general situa-
145 tions.

146 *2.3. Variational approach for domain coupling*

147 Unlike geometric design, where high continuity basis functions along the
148 intersections of neighboring patches are required for the construction of high
149 quality surface; in analysis, these strong point-wise constraints are unnec-
150 essarily rigorous, a good approximation of PDEs can be made even if these
151 constraints are applied in the weak sense. Moreover, the non-conforming
152 multi-patch coupling is allowed, which maintains the flexibility for the choice
153 of meshes when multi-patch discretization is needed. Mathematically, the er-
154 ror estimation of the non-conforming finite element approximation is based on
155 Strang's lemma [21, 85], which says that for the non-conforming discretized
156 PDEs, the distance between exact solution to the discrete one is bounded by
157 the sum of the approximation error and the consistency error. The approx-
158 imation error measures the failure of discretized finite dimensional space to
159 capture the exact solution, while the consistency error measures the incon-
160 sistency between the exact equation and the discretized equation. Various
161 methods have been developed to eliminate the consistency error and recover
162 optimal convergence, among them are the mortar method (Lagrange multi-
163 plier method), stabilized Lagrange multiplier method, the Nitsche's method
164 and the discontinuous Galerkin (dG) method.

To clearly demonstrate these methods, we consider the following Poisson

problem with homogenous Dirichlet boundary conditions

$$\begin{aligned} -\Delta u &= f, && \text{in } \Omega \\ u &= 0, && \text{on } \partial\Omega \end{aligned} \quad (1)$$

where Ω denote a bounded open domain in \mathbb{R}^d , $d = 2$ or 3 being the dimension of the problem and its boundary is denoted by $\partial\Omega$, in order to simplify the presentation we restrict ourselves to the case of two-dimensional computational domain. The weak form of Equation (1) reads as follow: Find $u \in H_0^1(\Omega)$ such that

$$a(u, v) = l(v), \quad \forall v \in H_0^1(\Omega), \quad (2)$$

where

$$\begin{aligned} a(u, v) &= \int_{\Omega} \nabla u \cdot \nabla v d\Omega, \\ l(v) &= \int_{\Omega} fv d\Omega. \end{aligned} \quad (3)$$

Using the fact that $C^0(\Omega) \subset H^1(\Omega)$, the weak solution can be approximated by considering a finite dimensional continuous function space. Now, we assume that the domain Ω is subdivided into K non-overlapping subdomains or patches Ω_k for $1 \leq k \leq K$, i.e.

$$\bar{\Omega} = \bigcup_{k=1}^K \bar{\Omega}_k \quad \text{and} \quad \Omega_k \bigcap \Omega_l = \emptyset \quad \forall k \neq l. \quad (4)$$

For simplicity, we only consider the case that the intersection of two patches is either empty or vertex or the entire edge, which rules out the possibility of hanging nodes. We denote the common interface of two neighboring subdomains $\Gamma_{kl} = \partial\Omega_k \cap \partial\Omega_l$ so that $\Gamma_{kl} = \emptyset$ if Ω_k is not a neighbor of Ω_l and define the skeleton $\mathbf{S} = \bigcup_{k,l \in K, k \neq l} \Gamma_{kl}$ as the union of all interfaces. A representative example of geometry is presented in Figure 1. We can associate each subdomain a bijective geometric mapping as

$$\mathbf{F}_k(\xi_k, \eta_k) : \hat{\Omega}_k \mapsto \Omega_k \in \mathbb{R}^d, \quad (5)$$

where $\hat{\Omega}_k$ is the parametric domain of k^{th} patch associated with coordinates (ξ_k, η_k) . For the simplicity and without loss of generality, we assume

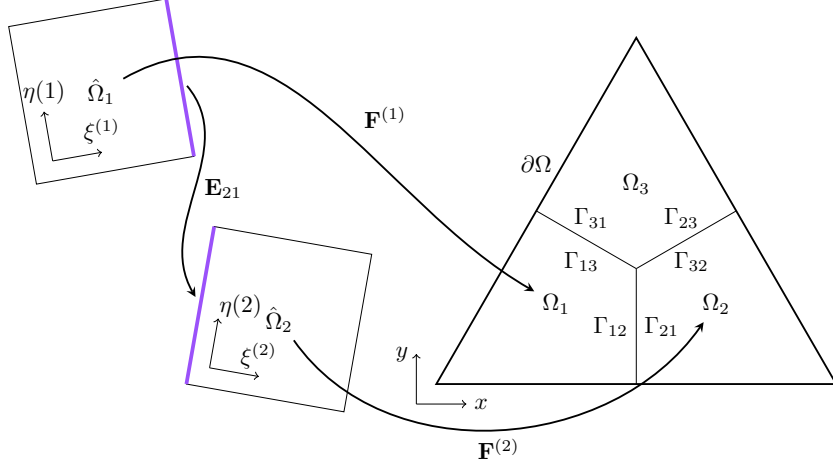


Figure 1: An example of domain decomposition, patches are defined on different parametric domains and are connected via geometric mapping.

¹⁸³ $\hat{\Omega}_k = [0, 1] \times [0, 1]$ for all patches. Due to the difference in the patch pa-
¹⁸⁴ rameterizations, a physical point on the interface can be mapped to different
¹⁸⁵ parametric domains with different coordinates. Owing to non-singular pa-
¹⁸⁶ rameterization, we can establish a bijective transformation from the shared
¹⁸⁷ edge of $\hat{\Omega}_k$ to that of $\hat{\Omega}_l$ by

$$\mathbf{E}_{kl} = (\mathbf{F}_l)^{-1} \circ \mathbf{F}_k. \quad (6)$$

¹⁸⁸

¹⁸⁹ For each Ω_k , we introduce the function space

$$H_*^1(\Omega_k) := \left\{ u \in H^1(\Omega_k) : u = 0 \text{ on } \partial\Omega \cap \partial\Omega_k \right\}, \quad (7)$$

¹⁹⁰ now we can define the broken Sobolev space

$$\mathcal{X} := \left\{ u \in L^2(\Omega) : u|_{\Omega_k} \in H_*^1(\Omega_k) \right\}. \quad (8)$$

¹⁹¹ Now, the question is how to approximate the weak solution of Equa-
¹⁹² tion (2) from a finite dimensional subspace of \mathcal{X} . Since functions in \mathcal{X} can be
¹⁹³ discontinuous on the skeleton \mathbf{S} , $a(u, u)$ is no longer coercive (or V-elliptic)
¹⁹⁴ on \mathcal{X} . As a result, directly using a finite dimensional subspace of \mathcal{X} to
¹⁹⁵ discretize Equation (2) will lead to a non-invertible stiffness matrix. Mod-
¹⁹⁶ ications to the weak form is needed, and we will review some of the most
¹⁹⁷ popular methods in this section.

198 2.3.1. Lagrange multiplier method

199 The Lagrange multiplier method (or sometimes called mortar method)
 200 is a domain decomposition technique that allows the coupling of different
 201 discretization schemes or of non-matching triangulation along interior inter-
 202 faces. The inter-element continuity condition is enforced weakly by Lagrange
 203 multipliers. For the Poisson problem, the C^0 continuity constraint is required
 204 on the intersections, in other words, the jump on the skeleton

$$[u]_{\Gamma_{kl}} := u_k - u_l = 0, \quad \forall \quad \Gamma_{kl} \in \mathbf{S}, \quad (9)$$

205 where $u_k = u|_{\Omega_k}$. In order to apply the constraint to the weak form, we
 206 introduce the potential energy functional:

$$\Pi(v) := \frac{1}{2}a(v, v) - l(v). \quad (10)$$

207 The Equation (2) is equivalent to the minimization problem:

$$\inf_{v \in H_0^1(\Omega)} \Pi(v). \quad (11)$$

208 Then, given a function space \mathcal{M} defined on the skeleton, a Lagrange multi-
 209 plier $\mu \in \mathcal{M}$ is used to add the constraint (9) to the potential energy func-
 210 tional (10), and the resulted the potential energy functional for the Lagrange
 211 multiplier method reads

$$\Pi_{LM}(v, \mu) := \Pi(v) + b(\mu, v), \quad (12)$$

212 where

$$b(\mu, v) = \sum_{\Gamma \in \mathbf{S}} \int_{\Gamma} \mu [u]_{\Gamma} d\Gamma. \quad (13)$$

213 The variational formulation of the Lagrange multiplier problem can be de-
 214 rived from the saddle point problem of the potential energy functional (12)

$$\inf_{v \in X} \sup_{\mu \in \mathcal{M}} \Pi_{LM}(v, \mu), \quad (14)$$

215 as, find $(u, \lambda) \in \mathcal{X} \times \mathcal{M}$ such that

$$\begin{cases} a(u, v) + b(v, \lambda) = l(v) & \forall v \in \mathcal{X}, \\ b(u, \mu) = 0 & \forall \mu \in \mathcal{M}. \end{cases} \quad (15)$$

216 The solution of the variational formulation is the infimum in v and the supre-
 217 mum in μ , in other words, it is still a minimization problem in terms of the
 218 primary variable v and any function that violate the constraint will be elim-
 219 inated by the Lagrange multiplier μ . This is the reason why it is called the
 220 saddle point problem. We also denote that the physical meaning of the La-
 221 grange multiplier μ for (12) is the flux of v over the skeleton. A comprehensive
 222 study of the mixed problem (15) can be found in [16].

223 In the discretized problem, for a given discrete space \mathcal{X}_h , the choice of
 224 the discrete Lagrange multiplier space \mathcal{M}_h plays a fundamental role for the
 225 stability of the saddle point problem and the optimality of the discretization
 226 scheme. To ensure the optimality, the function space for Lagrange multiplier
 227 should be judiciously chosen so that the consistency error should converges
 228 at the same rate as that of the approximation error. The feasibility of the
 229 discrete space pair $\mathcal{X}_h \times \mathcal{M}_h$ can be measured by the inf-sup test. The inf-sup
 230 condition is also refered to as the Ladyzhenskaya-Babuska-Brezzi condition
 231 (or simply LBB). It is a crucial condition to ensure the solvability, stabil-
 232 ity and optimality of a mixed problem. For the problem (15), the inf-sup
 233 condition is [16], for $v \neq 0$ and $\mu \neq 0$

$$\inf_{\mu \in \mathcal{M}} \sup_{v \in \mathcal{X}} \frac{|b(v, \mu)|}{\|v\|_{\mathcal{X}} \|\mu\|_{\mathcal{M}}} \geq \beta > 0. \quad (16)$$

234 Since the approximation error of problem (15) is given as

$$\|u - u^h\|_{\mathcal{X}} + \|\lambda - \lambda^h\|_{\mathcal{M}} \leq C \left(\inf_{u^h \in \mathcal{X}^h} \|u - u^h\|_{\mathcal{X}} + \inf_{\lambda^h \in \mathcal{M}^h} \|\lambda - \lambda^h\|_{\mathcal{M}} \right), \quad (17)$$

235 where C is a constant that depends on variables including β but is inde-
 236 pendent of the mesh size h . Hence, in a discretized problem, the inf-sup
 237 condition requires the variable β to be a constant that is independent of the
 238 mesh size.

239 It is well-known that in order to satisfy the LBB-condition a number of
 240 possible natural choices for the approximation space pair $\mathcal{X}_h \times \mathcal{M}_h$ must be
 241 discarded. In particular, the trace space of slave side, specially convenient
 242 from the computational point of view, often do not satisfy the LBB-condition
 243 and can activate pathologies such as spurious oscillations. To remedy this
 244 problem, the most widely used method in the finite element framework is
 245 reducing the dimension of Lagrange multiplier space by two (for 2nd order
 246 PDEs). Specifically, the degree of Lagrange multiplier basis functions at both

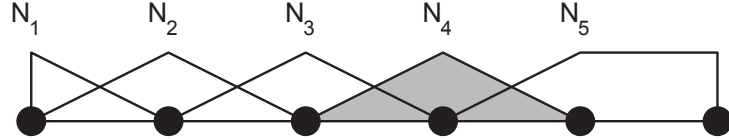


Figure 2: Lagrange multiplier basis functions for the piecewise linear elements, modification on the right end (from Zienkiewicz [94]).

247 ends are reduced by one. This modification has been sucessfully adopted in
 248 [14, 13, 7, 10, 8, 66, 61, 9]. An example of the modified Lagrange multiplier
 249 basis functions are illustrated in Figure 2, where the basis function N_5 is
 250 constant in the right end.

251 In the context of Isogeometric Analysis, the patch coupling problem has
 252 been firstly studied by Hesch and Betsch [48], where the coupling of La-
 253 grangian elements and NURBS elements for 3D nonlinear elastic problem
 254 is validated. To avoid an over constrained linear system, Hesch and Betsch
 255 used a linear Lagrange multiplier space for higher order NURBS coupling. In
 256 [22], the choice of the Lagrange multiplier space has been extensively studied,
 257 it testifies that for equal order pairing, a local degree reduction at extraor-
 258 dinary vertices is required, and another possibility is reducing the degree of
 259 Lagrange multiplier space by two compared to the trace space of slave side.
 260 These choices of Lagrange multiplier spaces are proven to be inf-sup stable
 261 by various numerical examples. In addition to the constraint on the inter-
 262 patch displacement, Bouclier *et al.* [20] considered the constraint on the
 263 traction and claimed that this strategy enables to present a C^1 behavior. In
 264 the numerical test, smoother displacement fields and smoother stress fields
 265 are observed.

266 Another drawback of the implementation of mortar methods is that most
 267 of them introduce Lagrange multipliers as additional variables to enforce
 268 interface constraints weakly, increasing the problem size. Moreover, different
 269 physical fields are involved in the weak form, deteriorating the conditioning
 270 of the global matrix if no appropriate pre-conditioner is applied (detailed
 271 discussion about preconditioning for saddle point problem can be found in
 272 [40, 11, 86]).

273 2.3.2. Dual mortar method

274 To circumvent the increase of problem size, we considering the minimiza-
275 tion problem

$$\inf_{v \in \mathcal{K}} \Pi(v), \quad (18)$$

276 where the function space $\mathcal{K} = \{v \in \mathcal{X} : b(v, \lambda) = 0, \forall \lambda \in \mathcal{M}\}$. The mini-
277 mization problem (18) is indeed equivalent to the saddle point problem (15),
278 the proof can be found in [16]. Note that, since $K \subset X$, the introduce of
279 Lagrange multiplier indeedly reduces the problem size of (18). Meanwhile,
280 the symmetric positive definite structure of the resulting stiffness matrix is
281 preserved. But the construction of the function space K is not a trivial task.

282 To reduce the cost of constructing the function space \mathcal{K} , we use the dual
283 basis functions of the trace space of the slave side as the discrete Lagrange
284 multiplier space. For a given basis function N_i , the dual basis function \hat{N}_j is
285 defined to satisfy

$$\int_{\Gamma} N_i \hat{N}_j d\Gamma = \delta_{ij} \int_{\Gamma} N_i d\Gamma, \quad (19)$$

286 where δ_{ij} is a Kronecker delta function. Of special interest, are biorthogonal
287 basis functions with compact support, especially

$$\text{supp } \hat{N}_i = \text{supp } N_i. \quad (20)$$

288 Due to the biorthogonality, the discrete bilinear form $b(v, \mu)$ forms a diagonal
289 matrix on the slave side, and forms a sparse matrix on the master side.
290 The function space \mathcal{K} can be formulated without additional efforts and all
291 the slave degree of freedom are eliminated in the resulting linear system.
292 Moreover, owing to the local support property the resulting stiffness matrix
293 is a symmetric positive definite sparse matrix. Thus, the dual basis functions
294 are very attractive in the perspective of computational efficiency.

295 Figure 3 shows an example of dual basis functions corresponding to the
296 basis functions in Figure 2. Again, order reduction is made at the right end.
297 The dual mortar method was first introduced in [91] for first order finite
298 element. This method has been extended to higher order degree elements in
299 [62], to three-dimensional problem in [92] and to contact problem [49, 75].

300 In isogeometric analysis framework, a master-slave type mortar method
301 has been suggested by Dornisch *et al.* [35], where the weakly applied con-
302 straint is represented as a master-slave relation and the the slave interface
303 degrees of freedom (DOF) can be condensed out of the global linear system.

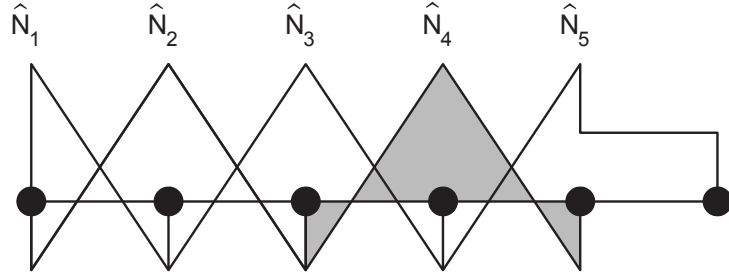


Figure 3: Dual Lagrange multiplier basis functions for the piecewise linear elements, modification on the right end (from Zienkiewicz [94]).

304 Recently, Dornisch *et al.* extended this research to multiple patch coupling in
 305 [37, 34], where different types of dual basis functions are applied as the basis
 306 of Lagrange multipliers. The numerical results demonstrate that the approx-
 307 imate dual basis functions yield accurate result and generate sparse global
 308 matrix due to the local support. The concept of dual mortar methods is also
 309 utilized in [82] for contact problem in Isogeometric analysis framework. Coox
 310 *et al.* [28] proposed an interesting approach to establish the master-slave mor-
 311 tar method and implemented this approach in [27] to form boundary element
 312 analysis on complex manifold. In this approach, the master-slave relation are
 313 formed by knot insertion algorithm and pseudo-inverse.

314 *2.3.3. Perturbed Lagrangian method*

315 Applying constraint by Lagrange multiplier leads to a saddle point prob-
 316 lem, of which the discrete Lagrange multiplier basis functions cannot be
 317 chosen independently of that of primal variable and special treatment is
 318 required on the cross point to ensure the solvability and optimality of the
 319 discretized system. The stiffness matrix for the discrete problem arising from
 320 the Lagrangian multiplier method always contains both positive and negative
 321 eigenvalues, for which iterative methods are known to be less efficient than for
 322 symmetric positive definite systems. To ensure the invertibility of the stiff-
 323 ness matrix, a quadratic penalty term is added to the energy functional (12),
 324 as

$$\Pi_{PLM}(v, \mu) := \Pi_{LM}(v, \mu) - \frac{1}{2\epsilon} \sum_{\Gamma \in S} \int_{\Gamma} \mu^2 d\Gamma, \quad (21)$$

325 where the penalty term is scaled by a parameter ϵ . The resulted func-
 326 tional (21) is referred to as perturbed Lagrangian and the last term is often

327 called stablization term. The resulted variational formulation is stated as

$$\begin{cases} a(u, v) + b(v, \lambda) = l(v) & \forall v \in \mathcal{X}, \\ b(u, \mu) - \frac{1}{\epsilon} \sum_{\Gamma \in \mathbf{S}} \int_{\Gamma} \mu \lambda d\Gamma = 0 & \forall \mu \in \mathcal{M}. \end{cases} \quad (22)$$

328 As $\epsilon \rightarrow \infty$, the solution obtained from (22) will converge to the solution ob-
329 tained by the classical Lagrange multiplier method. For $0 < \epsilon < \infty$, any solu-
330 tion that inconsistent with the constraint will not be fully prohibited, but will
331 be penalized by the stability term. And the rank of discrete stiffness matrix is
332 preserved no matter whether the discrete space pair $\mathcal{X}_h \times \mathcal{M}_h$ fulfills the inf-
333 sup condition or not. However, for a moderate ϵ , the perturbed Lagrangian
334 method is inconsistent with the classical Lagrange multiplier method, and
335 the increase of ϵ will deteriorate the conditioning of stiffness matrix.

336 The perturbed Lagrangian method has been utilized in [83] for contact
337 problem and [36, 1] for domain decomposition problem in isogeometric anal-
338 ysis framework.

339 2.3.4. Stabilized Lagrange multiplier method

340 To fully circumvent the inf-sup condition for imposing Dirichlet boundary
341 by Lagrange multiplier, Barbosa et. al. [3] added a new penalty like term
342 to the energy functional (12) to enhance the stability. Unlike perturbed
343 Lagrangian method where the penalty term is inconsistent with the original
344 problem, the new term proposed by Barbosa maintaining the consistency.
345 The energy functional of stablized Lagrange multiplier method is given as

$$\Pi_{SLM}(v, \mu) := \Pi_{LM}(v, \mu) - \sum_{\Gamma \in \mathbf{S}} \frac{h}{2\gamma} \int_{\Gamma} (\mu + \left\{ \frac{\partial v}{\partial n} \right\})^2 d\Gamma, \quad (23)$$

346 where n is the normal vector of the interface, h is the mesh size on the
347 intersection, γ is a user defined constant, the average operator

$$\{u\}_{\Gamma_{kl}} := \frac{1}{2} u_k + \frac{1}{2} u_l. \quad (24)$$

348 Since the physical meaning of the Lagrange multiplier is the flux on the
349 intersection, the stabilization term in (23) is consistent with the original
350 problem. The resulted variational formulation is stated as

$$\begin{cases} a(u, v) + b(v, \lambda) - \frac{h}{\gamma} \sum_{\Gamma \in \mathbf{S}} \int_{\Gamma} \frac{\partial v}{\partial n} (\lambda + \left\{ \frac{\partial u}{\partial n} \right\}) d\Gamma = l(v) & \forall v \in \mathcal{X}, \\ b(u, \mu) - \frac{h}{\gamma} \sum_{\Gamma \in \mathbf{S}} \int_{\Gamma} \mu (\lambda + \left\{ \frac{\partial u}{\partial n} \right\}) d\Gamma = 0 & \forall \mu \in \mathcal{M}. \end{cases} \quad (25)$$

351 The stabilization parameter γ needs to be carefully chosen. If γ is too large,
 352 the method degrades to a penalty-type method, with sub-optimal accuracy
 353 in the asymptotic limit. If γ is too small, the method becomes unstable.
 354 Recall the trace inequality

$$\|h^{\frac{1}{2}} \frac{\partial u}{\partial n}\|_{\partial\Omega_k}^2 \leq C \|\nabla u\|_{\Omega_k}^2. \quad (26)$$

355 It has been shown [51] that the mixed formulation (25) fulfills the inf-sup
 356 condition if $\gamma > 2C$. The constant C can be approximated by discretize
 357 the norms in the inequality (26) and solve the resulting discrete eigenvalue
 358 problem.

359 It has been demonstrated that there is a close connection with the sta-
 360 blized Lagrange multiplier method and Nitsche's method in the context of
 361 setting the Dirichlet boundary conditions [84] and in the context of domain
 362 decomposition [47, 46, 51]. Tur et. al. [88] utilized this method to solve
 363 both small and large deformation contact problems and obtained optimal
 364 convergence rate for linear elements. To our knowledge, this method has not
 365 been applied in the isogeometric analysis framework yet.

366 2.3.5. Discontinuous Galerkin method

367 Discontinuous Galerkin method (or Nitsche's method) was introduced in
 368 1971 [70] for handling Dirichlet boundary conditions in the weak sense. Dis-
 369 continuous Galerkin method resembles a mesh-dependent penalty method.
 370 Unlike the standard penalty method, which is not consistent unless the
 371 penalty coefficient goes to infinity, discontinuous Galerkin method is consis-
 372 tent with the original problem. Moreover, no additional unknown (Lagrange
 373 multiplier) is needed and no discrete inf-sup condition must be fulfilled, con-
 374 trarily to mixed methods. Meanwhile, additional term are added into the
 375 weak form to ensure the ellipticity of the problem.

376 To develop the weak form of discontinuous Galerkin method for homoge-
 377 neous Poisson problem, we start by multiplying (1) by a test function $v \in X$
 378 and integrating by parts, we obtain

$$a(u, v) - \sum_{\Gamma \in \mathbf{S}} \int_{\Gamma} \left\{ \frac{\partial u}{\partial n} \right\} [v] d\Gamma = l(v). \quad (27)$$

379 However, if we consider the right-hand side as a bilinear form, it is not
 380 coercive. In other words, this problem is not well-posed, since coercive implies

381 the uniqueness of solution. Meanwhile, this bilinear form is not symmetric.
 382 To recover the symmetry and coercivity of the bilinear form, additional terms
 383 are needed. To maintain the consistency, the added terms must vanish for
 384 the true solution. This lead to the following weak form: find $u \in X$ such
 385 that

$$a(u, v) - \sum_{\Gamma \in \mathbf{S}} \int_{\Gamma} \left\{ \frac{\partial u}{\partial n} \right\} [v] d\Gamma - \epsilon \sum_{\Gamma \in \mathbf{S}} \int_{\Gamma} \left\{ \frac{\partial v}{\partial n} \right\} [u] d\Gamma + \\ \sum_{\Gamma \in \mathbf{S}} \frac{\gamma}{h} \int_{\Gamma} [u] [v] d\Gamma = l(v) \quad \forall v \in \mathcal{X}. \quad (28)$$

386 Since $[u] = 0$ on the intersections, the above formulation is consistent with (27).
 387 Furthermore, and as already stated in [76] the parameter ϵ can be set to some
 388 particular values, namely:

- 389 • For $\epsilon = +1$, the resulting method is called the symmetric interior
 390 penalty Galerkin (SIPG) method. The stiffness matrix of SIPG is sym-
 391 metric.
- 392 • If $\epsilon = 0$, we obtain the incomplete interior penalty Galerkin (IIPG)
 393 method. It involves only a few terms and is of easiest implementation.
- 394 • If $\epsilon = -1$, the resulting method is called the nonsymmetric interior
 395 penalty Galerkin (NIPG) method. It admits one unique solution and
 396 converges optimally irrespectively of the value of $\gamma > 0$.

397 For $\epsilon = 0$ and $\epsilon = +1$, the bilinear form is coercive if $\gamma > C$ and $\gamma > 2C$,
 398 respectively [76]. Similar to the stablized Lagrange multiplier method, the
 399 discontinuous Galerkin method also requires to solve an eigenvalue problem
 400 to determine the value of γ .

401 Discontinuous Galerkin method has been widely studied in various as-
 402 pects, including imposing boundary condition [46], domain decomposition
 403 [6] and contact problem [25]. In the field of Isogeometric analysis, Discon-
 404 tinuous Galerkin method has been utilized to imposing Dirichlet boundary
 405 condition for trimmed spline meshes [39]. The first article discussing discon-
 406 tinuous Galerkin method based domain decomposition strategy was written
 407 by Apostolatos *et al.* [2]. Nguyen *et al.* extended it to three-dimensional
 408 problems in [69]. Guo *et al.* [45] proposed a Nitsche's method for cou-
 409 pling Kirchhoff-Love NURBS shell patches. Since the governing equation for

Table 1: Property comparison of Lagrange multiplier, dual mortal, perturbed Lagrange multiplier, stablized Lagrange multiplier and discontinuous Galerkin methods.

Methods	well-defined	inf-sup	symmetry	positive definite	size
Lagrange multiplier	depends	depends	yes	no	enlarged
Dual mortar	yes	depends	yes	yes	reduced
Perturbed Lagrange multiplier	yes	depends	yes	no	enlarged
Stabilized Lagrange multiplier	depends	yes	yes	no	enlarged
Discontinuous Galerkin	depends	yes	depends	yes	same

Table 1: Property comparison of Lagrange multiplier, dual mortal, perturbed Lagrange multiplier, stablized Lagrange multiplier and discontinuous Galerkin methods .

410 Kirchhoff-Love shell is 4-th order PDE, C^1 continuity constraint in imposed
 411 weakly in the method.

412 Although discontinuous Galerkin method does not introduce additional
 413 DOF and does not need the judicious choice of mutiplier function space,
 414 the value of the constants in the stablizing term need to be determined.
 415 Normally, they are determined by solving a eigenvalue problem on the domain
 416 of the combination of all intersections, which leads to extra computational
 417 cost. Meanwhile, the additional stablizing terms reduce the sparsity of the
 418 global linear system. For higher order PDEs, discontinuous Galerkin method
 419 becomes more complex as higher order derivatives exists in the tractions.

420 A comparison of the variational coupling methods discussed above is
 421 shown in Table. 1.

422 3. Research Objectives

423 My dissertation research focuses on the construction of NURBS basis
 424 functions among multi-patches that are analysis-suitable for 4th order PDEs.
 425 The coupling constraints are applied weakly by using the dual mortar method.
 426 The dual basis functions are constructed based on the Bézier probjective
 427 technology proposed in [87].

428 4. Preliminaries

429 This section provides the formulation of univariate basis functions, its
 430 extention to higher dimensional space, and representations of geometries in
 431 the context of Isogeometric Analysis. For a detailed explanation we refer to.

432 4.1. Univariate B-spline basis functions

433 A univariate B-spline is piecewise polynomial curve represented as a linear
 434 combination of B-spline basis functions. Basis functions of p^{th} order B-spline
 435 with n degrees of freedom can be defined by a non-decreasing set of real
 436 numbers

$$\Xi = \{\xi_1, \xi_2, \dots, \xi_{n+p+1}\}, \quad (29)$$

which is called knot vector. B-splines that are interpolatory at the ends can be achieved by requiring the multiplicity of $p + 1$ for the first and the last knot. Associated B-spline basis functions are defined using the Cox-de Boor recursion formula:

$$N_{i,0}(\xi) = \begin{cases} 1 & \xi_i \leq \xi \leq \xi_{i+1} \\ 0 & \text{otherwise} \end{cases} \quad (30)$$

$$N_{i,p}(\xi) = \frac{\xi - \xi_i}{\xi_{i+p} - \xi_i} N_{i,p-1}(\xi) + \frac{\xi_{i+p+1} - \xi}{\xi_{i+p+1} - \xi_{i+1}} N_{i+1,p-1}(\xi) \quad (31)$$

437 4.2. Univariate NURBS basis functions

438 The univariate Non-Uniform Rational B-spline (NURBS) can describe
 439 objects that cannot be represented by polynomial basis, such as circular arcs.
 440 NURBS are built from B-splines by dividing each B-spline basis functions by
 441 a weight function

$$W(\xi) = \sum_{j=1}^n w_j N_{j,p} \quad (32)$$

442 and multiplying each B-spline basis functions by the associated weight coeffi-
 443 cient for the partition of unity. Thus, the NURBS basis functions are defined
 444 as:

$$R_{i,p}(\xi) = \frac{w_i N_{i,p}}{W(\xi)} \quad (33)$$

445 4.3. Multivariate basis functions

446 For higher dimensional spaces, the B-spline and NURBS basis functions
 447 can be formed by the Kronecker product of vectors of univariate basis func-
 448 tions. For a two-dimensional parametric space, given polynomial orders of
 449 p_ξ, p_η and degrees of freedom n_ξ, n_η in ξ, η direction, the bivariate B-spline
 450 basis functions are defined as:

$$N_{a,\mathbf{p}}(\xi, \eta) = N_{i,p_\xi}(\xi) N_{j,p_\eta}(\eta), \quad (34)$$

⁴⁵¹ where the index a is defined by the map

$$a = n_\eta i + j. \quad (35)$$

⁴⁵² The bivariate NURBS basis functions are defined as

$$R_{a,\mathbf{p}}(\xi, \eta) = \frac{w_a N_{a,\mathbf{p}}}{\sum_{i=1}^n w_i N_{i,\mathbf{p}}}, \quad (36)$$

⁴⁵³ where $n = n_\xi \times n_\eta$. With some abuse of notation, we will drop the dependency
⁴⁵⁴ on the polynomial oder and use N_i to denote both NURBS basis functions
⁴⁵⁵ and B-spline basis functions in the rest of the paper.

⁴⁵⁶ 5. Weak- C^1 coupling for two-patch planar domains

⁴⁵⁷ To ground our approach in a practical example, we consider a biharmonic
⁴⁵⁸ problem on a two-patch planar domain, as demonstrated in Figure. 4. The
⁴⁵⁹ domain Ω is decomposed to the slave subdomain Ω_s (with finer mesh on the
⁴⁶⁰ interface) and the master subdomain Ω_m (with coarser mesh on the interface).

In order of focusing on the coupling algorithm itself, we assume the boundaries that neighboring to the common intersection to be homogeneous Neumann boundaries (north and south of Ω_s and east and west of Ω_m) and the rest to be homogeneous Dirichlet boundaries (west of Ω_s and south of Ω_m), denoted by Γ_N and Γ_D respectively. Then, the strong form of the two-patch biharmonic boundary value problem writes:

$$\begin{aligned} \Delta^2 u &= f, \quad \text{in } \Omega, \\ u &= \frac{\partial u}{\partial \mathbf{n}} = 0, \quad \text{on } \Gamma_D, \\ \Delta u &= \frac{\partial \Delta u}{\partial \mathbf{n}} = 0, \quad \text{on } \Gamma_N. \end{aligned} \quad (37)$$

⁴⁶¹ 5.1. Continuity constraints

The weak solution of the biharmonic problem (37) is in the space $H^2(\Omega)$. Due to the inclusion $C^1(\Omega) \subset H^2(\Omega)$, we can use C^1 -continuous functions to approximate the solution. For the two multi-patch domain, constraints

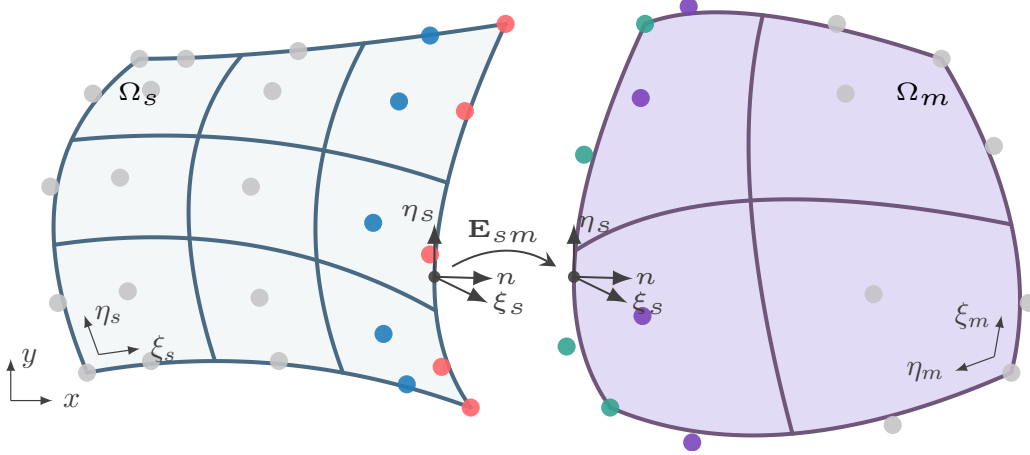


Figure 4: A two-patch planar domain constituted by Ω_m and Ω_s .

should be added to compromise the discontinuity along the intersection. In general, the following two constraints are requested for u to be C^1 -continuous

$$[u]_{\Gamma_{sm}} = 0, \quad (38a)$$

$$\left[\frac{\partial u}{\partial \mathbf{n}} \right]_{\Gamma_{sm}} = 0, \quad \text{with } \mathbf{n} = \mathbf{n}_s = -\mathbf{n}_m \quad (38b)$$

where \mathbf{n}_k is the outward normal direction of $\partial\Omega_k$.

Whereas the constraint (38a) can easily fit into the framework of dual mortar method, the constraint (38b) can not be directly imposed. First of all, the existence of dual basis functions of $\frac{\partial N_i}{\partial \mathbf{n}}|_{\Gamma_{sm}}$ is doubtful. Even if they exist, as they are biorthogonal to the normal derivative of NURBS, their formulation must depend on the parameterization of Γ_{sm} , which violates the virtue of simplicity of dual basis functions. Hence, we need the following result, of which the derivatives are defined in the parametric domain and the dual basis functions can be formulated in an elegant manner.

Lemma 1. *Given two differentiable bijective geometric mappings $\mathbf{F}_s: \hat{\Omega}_s \rightarrow \Omega_s$ and $\mathbf{F}_m: \hat{\Omega}_m \rightarrow \Omega_m$, a C^0 -continuous function u is C^1 -continuous in the physical domain if and only if*

$$\left[\frac{\partial u}{\partial \xi_s} \right]_{\Gamma_{sm}} = 0 \text{ and } \left[\frac{\partial u}{\partial \eta_s} \right]_{\Gamma_{sm}} = 0. \quad (39)$$

Proof. It suffices to consider two neighboring patches as shown in Figure 4. u is C^0 -continuous function implies $\left[\frac{\partial u}{\partial \eta_s} \right]_{\Gamma_{sm}} = 0$. For the C^1 -continuity of u ,

we have the following relation

$$\begin{cases} \frac{\partial u_s}{\partial x} = \frac{\partial u_m}{\partial x} \\ \frac{\partial u_s}{\partial y} = \frac{\partial u_m}{\partial y} \end{cases} \xrightarrow{[\frac{\partial u}{\partial \eta_s}]_{\Gamma_{sm}}=0} \begin{cases} \frac{\partial u_s}{\partial \xi_s} \frac{\partial \xi_s}{\partial x} = \frac{\partial u_m}{\partial \xi_s} \frac{\partial \xi_s}{\partial x} \\ \frac{\partial u_s}{\partial \xi_s} \frac{\partial \xi_s}{\partial y} = \frac{\partial u_m}{\partial \xi_s} \frac{\partial \xi_s}{\partial y} \end{cases} \quad \text{on } \Gamma_{sm} \quad (40)$$

⁴⁷⁴ Since the geometric mapping \mathbf{F}_s is bijective, there exist an inverse mapping
⁴⁷⁵ \mathbf{F}_s^{-1} and $\det(\mathbf{F}_s^{-1}) \neq 0$. Thus, $[\frac{\partial u}{\partial \xi_s}]_{\Gamma_{sm}} = 0$. This concludes the proof. \square

The derivatives of u_m w.r.t. ξ_s and η_s can be obtained following the chain rule, as

$$\begin{bmatrix} \frac{\partial u_m}{\partial \xi_s} \\ \frac{\partial u_m}{\partial \eta_s} \end{bmatrix} = J(\mathbf{E}_{sm})^T \cdot \begin{bmatrix} \frac{\partial u_m}{\partial \xi_m} \\ \frac{\partial u_m}{\partial \eta_m} \end{bmatrix}, \quad (41)$$

⁴⁷⁶ where $J(\cdot)$ is the Jacobian of the mapping in the argument. The Jacobian of
⁴⁷⁷ the composition mapping \mathbf{E}_{sm} can be written as

$$J(\mathbf{E}_{sm}) = J((\mathbf{F}_m)^{-1} \circ \mathbf{F}_s) = J((\mathbf{F}_m)^{-1}) \cdot J(\mathbf{F}_s) = J(\mathbf{F}_m)^{-1} \cdot J(\mathbf{F}_s). \quad (42)$$

⁴⁷⁸ 5.2. Lagrange multiplier formulation and dual mortar formulation

We introduce two Lagrange multiplier spaces: M_0 is devoted to the C^0 constraint (38a) and M_1 is devoted to the C^1 constraint (39). The Lagrange multiplier formulation of the weak problem of (37) reads: find $u \in X_b$, $\lambda_0 \in M_0$ and $\lambda_1 \in M_1$ such that:

$$\begin{cases} a_b(u, v) + b_0(\lambda_0, v) + b_1(\lambda_1, v) = l(v), & \forall v \in X_b; \\ b_0(\mu_0, u) = 0, & \forall \mu_0 \in M_0; \\ b_1(\mu_1, u) = 0, & \forall \mu_1 \in M_1; \end{cases} \quad (43)$$

with

$$a_b(u, v) = \int_{\Omega} \Delta u \Delta v d\Omega, \quad (44)$$

$$b_0(\mu, u) = \int_{\Gamma_{sm}} \mu [u]_{\Gamma} d\Gamma, \quad (45)$$

$$b_1(\mu, u) = \int_{\Gamma_{sm}} \mu \left[\frac{\partial u}{\partial \xi_s} \right]_{\Gamma} d\Gamma. \quad (46)$$

⁴⁷⁹ The broken Sobolev space for the biharmonic problem is given as

$$\mathcal{X}_b := \{u \in L^2(\Omega) : u|_{\Omega_k} \in H_*^2(\Omega_k)\}, \quad (47)$$

480 with

$$H_*^2(\Omega_k) := \left\{ u \in H^2(\Omega_k) : u = 0 \text{ and } \frac{\partial u}{\partial \mathbf{n}} = 0 \text{ on } \partial\Gamma_D \cap \partial\Omega_k \right\}. \quad (48)$$

481 By moving the constraints from the problem statement to the definition of the
482 trial and test function spaces, we obtain the following variational problem:
483 find $u \in \mathcal{K}_b$, such that

$$a_b(u, v) = l(v), \quad \forall v \in \mathcal{K}_b, \quad (49)$$

484 where

$$\mathcal{K}_b := \{u \in \mathcal{X}_b : b_0(u, \mu_0) = 0 \text{ and } b_1(u, \mu_1) = 0 \quad \forall (\mu_0, \mu_1) \in \mathcal{M}_0 \times \mathcal{M}_1\}. \quad (50)$$

485 On one hand, the absence of the Lagrange multipliers λ_0 and λ_1 reduces the
486 size of the discretized problem and recovers the symmetric positive definite
487 structure of the stiffness matrix. As a result, efficient iterative solvers can be
488 applied for the problem. On the other hand, in the standard formalism, \mathcal{M}_0
489 and \mathcal{M}_1 are discretized by the trace of one side of the intersection so that
490 the construction of \mathcal{K}_b^h requires a factorization of a global constraint matrix,
491 which is not a trivial task.

492 However, in the following section, we will show that, with the help of dual
493 basis functions, the discretized function space \mathcal{K}_b^h can be formulated in an
494 elegant manner.

495 5.3. Finite element approximation

496 Suppose that $\mathcal{X}_b^h \subset \mathcal{X}_b$, $\mathcal{M}_0^h \subset \mathcal{M}_0$ and $\mathcal{M}_1^h \subset \mathcal{M}_1$ are finite-dimensional
497 linear subspaces of the Hilbert spaces \mathcal{X}_b , \mathcal{M}_0 , and \mathcal{M}_1 ; we study the finite
498 element approximation of the abstract problem (43).

Assumption 1. All bilinear functionals are bounded; i.e., there exist positive constants C_a , C_{b_0} and C_{b_1} such that

$$\begin{aligned} |a_b(u, v)| &\leq C_a \|u\|_{H^2} \|v\|_{H^2}, & \forall u, v \in \mathcal{X}_b, \\ |b_0(\mu_0, u)| &\leq C_{b_0} \|\mu_0\|_{L^2} \|u\|_{H^2}, & \forall \mu_0 \in \mathcal{M}_0, u \in \mathcal{X}_b, \\ |b_1(\mu_1, u)| &\leq C_{b_1} \|\mu_1\|_{L^2} \|u\|_{H^2}, & \forall \mu_1 \in \mathcal{M}_1, u \in \mathcal{X}_b. \end{aligned} \quad (51)$$

499 *Assumption 2.* In addition, we assume that the bilinear functional $a_b(\cdot, \cdot)$ is
500 coercive on \mathcal{K}_b , i.e.,

$$\exists c_a > 0 \quad s.t. \quad \forall v^h \in \mathcal{K}_b^h, \quad a_b(v^h, v^h) \geq c_a \|v^h\|_{H^2} \quad (52)$$

501 Following standard techniques [21], we now obtain a bound on the error
 502 between u and u^h in term of the best approximation errors, which can be
 503 considered as Céa's lemma for mixed problems.

504 *Theorem 1.* Under the above assumptions, there exists a unique solution
 505 $u^h \in \mathcal{K}_b^h$ satisfies (49). Furthermore,

$$\|u - u^h\|_{H^2} \leq \left(1 + \frac{C_a}{c_a}\right) \inf_{v^h \in \mathcal{K}_b^h} \|u - v^h\|_{H^2} + \frac{C_b}{c_a} \left(\inf_{\mu_0^h \in \mathcal{M}_0^h} \|\lambda_0 - \mu_0^h\|_{L^2} + \inf_{\mu_1^h \in \mathcal{M}_1^h} \|\lambda_1 - \mu_1^h\|_{L^2} \right), \quad (53)$$

506 where $C_b = \max(C_{b_0}, C_{b_1})$.

507 Hence, the error of finite element approximations in broken $H^2(\Omega)$ norm
 508 are bounded by the best approximation error of $v^h \in \mathcal{K}_b^h$ in broken $H^2(\Omega)$
 509 norm and $\mu_0^h \in \mathcal{M}_0^h$, $\mu_1^h \in \mathcal{M}_1^h$ in $L^2(\Gamma)$ norm. In general, the approximation
 510 ability of p^{th} order piecewise polynomial in \mathcal{X}_b^h is given by

$$\|u - u^h\|_{H^s} \leq Ch^{p+1-s}. \quad (54)$$

511 where C is a constant that is independent of the mesh size h . To transform
 512 approximation estimates in \mathcal{K}_b^h into standard approximation estimates in \mathcal{X}_b^h ,
 513 we need the following assumption:

Assumption 3. Furthermore, we assume that the bilinear functionals $b_0(\cdot, \cdot)$
 and $b_1(\cdot, \cdot)$ are inf-sup stable in the discretized formulation, i.e., there exist
 positive constants β_0 and β_1 independent of the mesh size such that

$$\inf_{\mu_0^h \in \mathcal{M}_0^h} \sup_{u^h \in \mathcal{X}_b^h} \frac{|b_0(\mu_0^h, u)|}{\|u^h\|_{H^2} \|\mu_0^h\|_{L^2}} \geq \beta_0, \quad (55)$$

$$\inf_{\mu_1^h \in \mathcal{M}_1^h} \sup_{u^h \in \mathcal{X}_b^h} \frac{|b_1(\mu_1^h, u)|}{\|u^h\|_{H^2} \|\mu_1^h\|_{L^2}} \geq \beta_1. \quad (56)$$

514 *Theorem 2.* Under the assumptions, we have that, for any $u \in \mathcal{K}_b$,

$$\inf_{v^h \in \mathcal{K}_b^h} \|u - v^h\|_{H^2} \leq \left(1 + \frac{C_b}{\beta}\right) \inf_{w^h \in \mathcal{X}_b^h} \|u - w^h\|_{H^2} \quad (57)$$

515 where $\beta = \min(\beta_0, \beta_1)$.

516 As can be seen, the optimality of $u^h \in \mathcal{K}_b^h$ requires the inf-sup stability of
 517 bilinear functional b_0 and b_1 . The analytical study of the inf-sup stability is

518 beyond the scope of this paper. Instead, we demonstrate the approximation
 519 ability of \mathcal{K}_b^h by directly conducting H^2 projection in different numerical
 520 examples.

521 Meanwhile, the approximation ability of the Lagrange multiplier spaces
 522 \mathcal{M}_0^h and \mathcal{M}_1^h also influence the optimality of the finite element approxima-
 523 tion. Whereas u is approximated in H^2 space, λ_0 and λ_1 are approximated in
 524 L^2 space. Hence, the optimality of the finite element approximation requires
 525 that both \mathcal{M}_0^h and \mathcal{M}_1^h are at least $p - 2$ complete, i.e., functions in \mathcal{M}_0^h and
 526 \mathcal{M}_1^h can exactly represent polynomials up to order $p - 2$.

527 *5.4. Discretization*

In order to approximate the solution of the variational problem, we use the NURBS basis functions $N_i^{(s)}$ $i \in I_s$ and $N_j^{(m)}$ $j \in I_m$ to discretize coupled patches Ω_s and Ω_m , respectively. An appropriate offset has been made so that there is no overlapping between index sets I_s and I_m (given n_s basis functions in Ω_s , we can assume the starting index in the index set I_m is $n_s + 1$). The discretized geometrical mappings are represented by

$$\mathbf{F}_s = \sum_{i \in I_s} \mathbf{P}_i^s N_i^s, \quad (58)$$

$$\mathbf{F}_m = \sum_{i \in I_m} \mathbf{P}_i^m N_i^m, \quad (59)$$

528 where the control points $\mathbf{P}_i^s, \mathbf{P}_i^m \in \mathbb{R}^2$. The same basis functions are also
 529 used to discretize the test function u in broken Sobolev space \mathcal{X}_b , as

$$u^h = \sum_{i \in I_s + I_m} U_i N_i, \quad (60)$$

with

$$N_i = \begin{cases} N_i^s, & i \in I_s; \\ N_i^m, & i \in I_m. \end{cases} \quad (61)$$

530 As compared to the standard formalism that utilizes the trace of the slave
 531 patch on the intersection as the discretization of Lagrange multipliers, in this
 532 research, we construct Lagrange multipliers by using Bézier dual basis. We
 533 first classify NURBS basis functions into five different kinds, as shown in
 534 Figure. 4, namely:

- 535 1. The basis functions $N_i^{(s)}$ such that $\text{supp}(N_i^{(s)}) \cap \Gamma_{sm} = \emptyset$ and $\text{supp}(\frac{\partial N_i^{(s)}}{\partial \xi_s}) \cap \Gamma_{sm} \neq \emptyset$, whose indices are in the index set I_i . (denoted by blue dots)
- 536 2. The basis functions $N_i^{(s)}$ such that $\text{supp}(N_i^{(s)}) \cap \Gamma_{sm} \neq \emptyset$, whose indices are in the index set I_{ii} . (denoted by red dots)
- 537 3. The basis functions $N_i^{(m)}$ such that $\text{supp}(N_i^{(m)}) \cap \Gamma_{sm} = \emptyset$ and $\text{supp}(\frac{\partial N_i^{(m)}}{\partial \xi_s}) \cap \Gamma_{sm} \neq \emptyset$, whose indices are in the index set I_{iii} . (denoted by green dots)
- 538 4. The basis functions $N_i^{(m)}$ such that $\text{supp}(N_i^{(m)}) \cap \Gamma_{sm} \neq \emptyset$, whose indices are in the index set I_{iv} . (denoted by purple dots)
- 539 5. All basis functions neither the supports of themselves nor the supports of their first order derivatives in ξ_s direction intersect with Γ_{sm} , whose indices are in the index set I_v . (denoted by grey dots)

540
541
542
543
544
545 For the basis functions of the second kind, their restrictions on the intersection Γ_{sm} are one dimensional NURBS basis functions $N_{i,p_\eta}^{(s)} i \in \{1, 2, \dots, n_\eta^s\}$ that are used to discretize the tensor-product domain Ω_s in η direction. In order to obtain an Identity matrix on the slave side of the discretized bilinear form b_0 , the associated dual basis functions of $N_{i,p_\eta}^{(s)}$ are used to discretize the Lagrange multiplier space \mathcal{M}_0 , as

$$\lambda_0^h = \sum_{i=1}^{n_\eta^s} \Lambda_i^0 \hat{N}_{i,p_\eta}^{(s)}. \quad (62)$$

552 For the basis functions of the first kind, the restrictions of their first order
553 derivatives on the intersection Γ_{sm} can be written as $c N_{i,p_\eta}^{(s)} i \in \{1, 2, \dots, n_\eta^s\}$,
554 with $c = N_{n_\xi^s-1,p_\xi}^{(s)}(1)$. Hence, the Lagrange multiplier space \mathcal{M}_1 can be
555 discretized by

$$\lambda_1^h = \sum_{i=1}^{n_\eta^s} \Lambda_i^1 \tilde{N}_i, \quad \text{with } \tilde{N}_i = \frac{1}{c} N_{i,p_\eta}^{(s)}. \quad (63)$$

556 We denote the basis functions in \mathcal{M}_0^h and \mathcal{M}_1^h as the dual basis functions of
557 the second and the first kinds of NURBS basis functions, respectively.

558 By substituting these NURBS approximations into the Lagrange multi-
559 plier formulation (43), we obtain the following linear system:

$$\begin{bmatrix} \mathbf{K} & \mathbf{B}^T \\ \mathbf{B} & \mathbf{0} \end{bmatrix} \begin{bmatrix} \mathbf{U} \\ \mathbf{\Lambda}_0 \\ \mathbf{\Lambda}_1 \end{bmatrix} = \begin{bmatrix} \mathbf{F} \\ \mathbf{0} \end{bmatrix}, \quad (64)$$

560 where \mathbf{K} and \mathbf{F} are the stiffness matrix and the load vector for the uncoupled
 561 problem, respectively. \mathbf{B} is the constraint matrix discretized from the bilinear
 562 forms b_0 and b_1 . In order to construct the finite element space \mathcal{K}_b^h , we need to
 563 solve the constraint matrix \mathbf{B} 's null space $\mathbf{C} = \ker(\mathbf{B})$. Since the structure of
 564 the constraint matrix \mathbf{B} depends on the index sets I_s and I_m and the ordering
 565 of Lagrange multiplier basis functions, without adding any constraints on the
 566 indices, we introduce two permutation matrices \mathbf{P}_c and \mathbf{P}_r (this step is not
 567 necessary from the implementation point of view, but is very convenient
 568 for the demonstration, especially for multi-patch problem). We define the
 569 column permutation matrix \mathbf{P}_c as

$$\begin{bmatrix} \mathbf{I}_i \\ \mathbf{I}_{ii} \\ \mathbf{I}_{iii} \\ \mathbf{I}_{iv} \\ \mathbf{I}_v \end{bmatrix} = \mathbf{P}_c \begin{bmatrix} \mathbf{I}_s \\ \mathbf{I}_m \end{bmatrix}, \quad (65)$$

570 where \mathbf{I}_i is the vector form of the index set I_i . For an appropriate row
 571 permutation matrix \mathbf{P}_r , the modified constraint matrix can be written in a
 572 partitioned form as

$$\mathbf{B}_p = \mathbf{P}_r \mathbf{B} \mathbf{P}_c^T = \begin{bmatrix} \mathbf{B}_1^1 & \mathbf{B}_1^2 & \mathbf{B}_1^3 & \mathbf{B}_1^4 & \mathbf{0} \\ \mathbf{0} & \mathbf{B}_2^2 & \mathbf{B}_2^3 & \mathbf{0} & \mathbf{0} \end{bmatrix}, \quad (66)$$

573 where \mathbf{B}_i^j corresponds to the contribution of the inner product of the basis
 574 functions of the j^{th} kind with the dual basis functions of the i^{th} kind. \mathbf{P}_r
 575 can be defined as a row permutation matrix such that the resulted block
 576 sub-matrices \mathbf{B}_1^1 and \mathbf{B}_2^2 are both identity matrices. Under a rank-preserving
 577 transformation \mathbf{T} , we can eliminate the block sub-matrix \mathbf{B}_1^2 , as

$$\mathbf{T}\mathbf{B}_p = \begin{bmatrix} & \mathbf{I} & \begin{array}{|c|c|c|c|} \hline & \mathbf{B}_1^3 - \mathbf{B}_1^2 \mathbf{B}_2^3 & \mathbf{B}_1^4 & \mathbf{0} \\ \hline & \mathbf{B}_2^3 & \mathbf{0} & \mathbf{0} \\ \hline \end{array} \end{bmatrix}. \quad (67)$$

578 We may now take

$$\mathbf{C}_p := \ker(\mathbf{B}_p) = \begin{bmatrix} \mathbf{B}_1^2 \mathbf{B}_2^3 - \mathbf{B}_1^3 & -\mathbf{B}_1^4 & \mathbf{0} \\ -\mathbf{B}_2^3 & \mathbf{0} & \mathbf{0} \\ \hline & \mathbf{I} & \end{bmatrix}. \quad (68)$$

⁵⁷⁹ Hence, the null space of \mathbf{B} can be taken as

$$\mathbf{C} = \mathbf{P}_c^T \mathbf{C}_p. \quad (69)$$

⁵⁸⁰ Now we can discretize functions in \mathcal{K}_b^h as

$$u^h = \mathbf{N}^T \mathbf{U}, \quad \text{with } \mathbf{U} = \mathbf{C} \tilde{\mathbf{U}}, \quad (70)$$

⁵⁸¹ where \mathbf{N} is the vector form of basis functions of \mathcal{X}_b^h , and $\tilde{\mathbf{U}}$ is the control
⁵⁸² point vector. By substituting the above discretization in the weak form (50),
⁵⁸³ we obtain the following linear system to be solved:

$$\mathbf{C}^T \mathbf{K} \mathbf{C} \tilde{\mathbf{U}} = \mathbf{C}^T \mathbf{F}. \quad (71)$$

⁵⁸⁴ Because of the biorthogonality of the NURBS basis functions and their dual
⁵⁸⁵ basis functions, the constrained solution spcae \mathcal{K}_b^h can be constructed very
⁵⁸⁶ efficiently, leading to a sparse, symmetric positive definite formulation.

⁵⁸⁷ 6. Weak- C^1 coupling for multi-patch planar domains

⁵⁸⁸ To generate complex geometries, we need to decompose domain to mul-
⁵⁸⁹ tiple patches. Unfortunately, we cannot apply directly the results of two-
⁵⁹⁰ patch coupling to this more general mortar situation. The main issue is
⁵⁹¹ the so-called cross points. For a multi-patch decomposition, at least three
⁵⁹² subdomains meet at an interior crosspoint and several interfaces can share
⁵⁹³ this cross point as a common endpoint (Figure. 5). If we use the discretized
⁵⁹⁴ Lagrange multipliers proposed in the previous section, owing to the presence
⁵⁹⁵ of cross points, some of the control points will serve as both slave points
⁵⁹⁶ (indices in I_1 and I_2) and master points (indices in I_3 and I_4). Hence, there
⁵⁹⁷ is no permutation matrices such that the constraint matrix \mathbf{B} can be mod-
⁵⁹⁸ ified to the form as equation (67), of which the null space can be found in
⁵⁹⁹ a trivial way. Even more, although the constraint matrices defined on each
⁶⁰⁰ interfaces are full row rank, the assembled constraint matrix \mathbf{B} may not be
⁶⁰¹ full row rank in most cases, which renders the linear system (64) to be rank
⁶⁰² deficient. As a result, either modifications to the Lagrange multipliers or to
⁶⁰³ the method itself is required so that the proposed method can be generalized
⁶⁰⁴ to a setting where a domain can be decomposed to an arbitrary number of
⁶⁰⁵ patches. Before we start this section, we would like to introduce the sixth
⁶⁰⁶ kind of NURBS basis function that associated with the cross point v , as

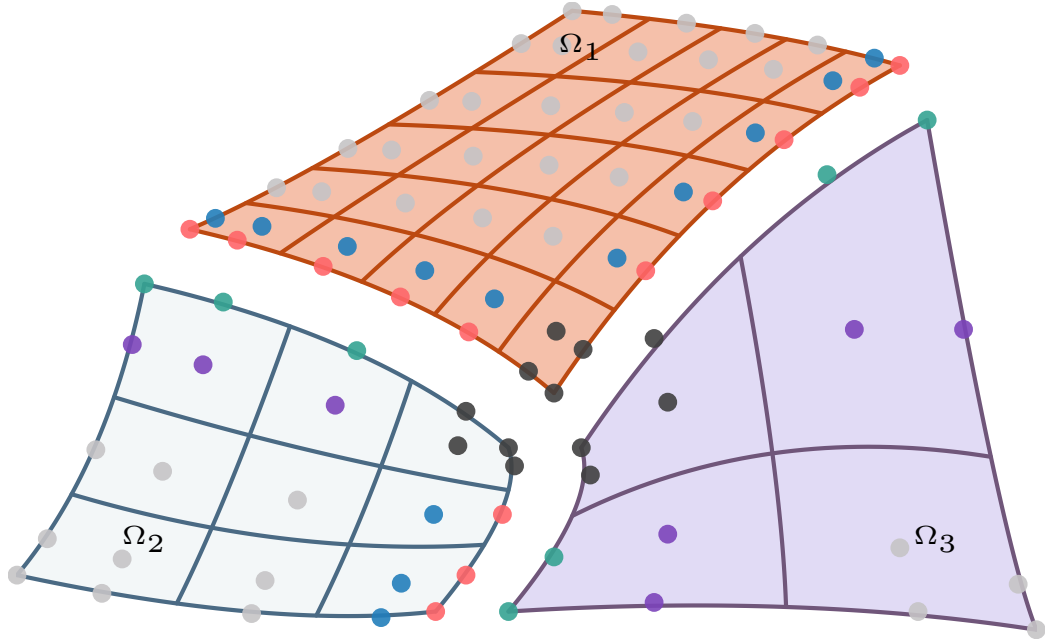


Figure 5: A three-patch planar domain constituted by Ω_1 , Ω_2 and Ω_3 .

- 607 6. The basis function N_i such that $\text{supp}(N_i) \cap v \neq 0$, or $\text{supp}(\frac{\partial N_i}{\partial \xi}) \cap v \neq$
608 0, or $\text{supp}(\frac{\partial N_i}{\partial \eta}) \cap v \neq 0$ or $\text{supp}(\frac{\partial^2 N_i}{\partial \xi \partial \eta}) \cap v \neq 0$, whose indices are in the
609 index set I_{vi} . (denoted by black dots in Figure. 5)
- 610 The rest five kinds of NURBS basis function remain the same except their
611 intersection with the sixth kind are excluded, that is

$$I_k = I_k - I_{vi} \bigcap I_k, \quad k \in \{i, ii, \dots, v\}. \quad (72)$$

- 612 The basis functions in \mathcal{M}_0^h and \mathcal{M}_1^h can be classified as the dual basis func-
613 tions of the NURBS basis function of the 1st, 2nd and 6th kind, respectively.
614 The domains on the two sides of each interface can still be considered as slave
615 and master based on the same rule as for the two-patch coupling case.

616 6.1. *Cross point modification*

617 Since using the discretization of Lagrange multipliers proposed for two-
618 patch coupling case directly results in over-constrained constraint matrix \mathbf{B}
619 for the control points round the crosspoints, we can remedy this issue by re-
620 ducing the dimension of the Lagrange multiplier spaces. Roughly speaking,

621 we have to remove the two degrees of freedom of the Lagrange multiplier
 622 spaces associated with each cross point so that the resulted Lagrange multi-
 623 plier spaces on each interface should have the same dimension as $\mathcal{X}_b^h|_{\Omega_s} \cap H_0^2(\Gamma_{sm})$.

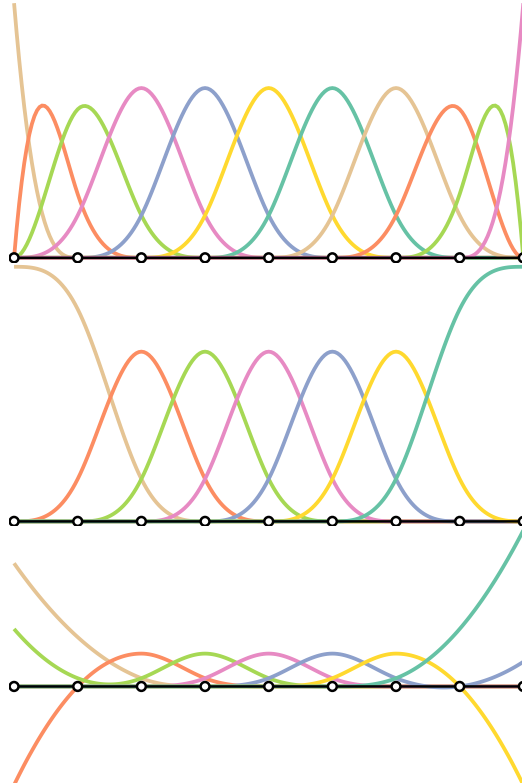


Figure 6: Quadratic basis functions and their cross point modifications. Top: original quadratic basis functions. Middle: coarsened basis functions. Bottom: degree reduced basis functions

624 This can be achieved by two ways: we can either coarse the mesh for the
 625 Lagrange multiplier in the neighborhood of the cross point, or reduce their
 626 polynomial degree in the neighborhood of the cross point. An example for
 627 quadratic 1-D B-spline basis functions is shown in Figure. 6. The coarsened
 628 basis functions are achieved by replacing the first three and last three basis
 629 functions by their summations, while we can construct degree reduced basis
 630 functions by reduce the polynomial degree of the first and last two elements
 631 by one while retaining the inter-element continuity.

632 Although the degree reduction is not a trivial task for dual basis, the
 633 summation trick can be applied to coarse dual basis functions. After the

634 coarsen procedure, the dual basis functions associated with the basis func-
 635 tions of 6th kind are all eliminated so that no inter-dependencies will happen
 636 in the neighborhood of the cross point. We can define a column permutation
 637 matrix

$$\begin{bmatrix} \mathbf{I}_i \\ \mathbf{I}_{ii} \\ \mathbf{I}_{iii} \\ \mathbf{I}_{iv} \\ \mathbf{I}_{vi} \\ \mathbf{I}_v \end{bmatrix} = \tilde{\mathbf{P}}_c \begin{bmatrix} \mathbf{I}_1 \\ \mathbf{I}_2 \\ \mathbf{I}_3 \end{bmatrix}. \quad (73)$$

638 With a suitable row permutation matrix $\tilde{\mathbf{P}}_r$, the constraint matrix \mathbf{B} can be
 639 modified as

$$\tilde{\mathbf{B}}_p := \tilde{\mathbf{P}}_r \mathbf{B} \tilde{\mathbf{P}}_c^T = \begin{bmatrix} \mathbf{B}_1^1 & \mathbf{B}_1^2 & \mathbf{B}_1^3 & \mathbf{B}_1^4 & \mathbf{B}_1^6 & \mathbf{0} \\ \mathbf{0} & \mathbf{B}_2^2 & \mathbf{B}_2^3 & \mathbf{0} & \mathbf{B}_2^6 & \mathbf{0} \end{bmatrix}, \quad (74)$$

640 with \mathbf{B}_1^1 and \mathbf{B}_2^2 be identity matrices. Hence, its null space can be found as

$$\tilde{\mathbf{C}}_p := \ker(\tilde{\mathbf{B}}_p) = \begin{bmatrix} \mathbf{B}_1^2 \mathbf{B}_2^3 - \mathbf{B}_1^3 & -\mathbf{B}_1^4 & -\mathbf{B}_1^6 & \mathbf{0} \\ -\mathbf{B}_2^3 & \mathbf{0} & -\mathbf{B}_2^6 & \mathbf{0} \\ \vdots & & \vdots & \\ \mathbf{I} & & & \end{bmatrix}. \quad (75)$$

641 Although the boundary modification by coarsening eliminates the inter-dependency
 642 in the neighborhood of cross points, numerical tests demonstrate sub-optimality.

6.2. Explicitly solve the null space

644 Instead of modifying the Lagrange multipliers, we can solve the null space
 645 of the over-constrained constraint matrix \mathbf{B} directly. Seveal matrix factoriza-
 646 tion methods can be used to solve the null space, including LU, QR, SVD. For
 647 example, a rank-revealing QR factorization over a rank-deficiency constraint
 648 matrix \mathbf{B} yields

$$\mathbf{B}\mathbf{P} = \mathbf{Q} \begin{bmatrix} \mathbf{R}_1 & \mathbf{R}_2 \\ \mathbf{0} & \mathbf{0} \end{bmatrix} \quad (76)$$

649 where \mathbf{P} is a permutation matrix, \mathbf{Q} is an unitary matrix, \mathbf{R}_1 is a upper
 650 triangular matrix and \mathbf{R}_2 is a rectangular matrix. The null space can be
 651 taken as

$$\ker(\mathbf{B}) = \mathbf{P} \begin{bmatrix} -\mathbf{R}_1^{-1} \mathbf{R}_2 \\ \mathbf{I} \end{bmatrix}. \quad (77)$$

652 However, this requires a factorization of the entire constraint matrix \mathbf{B} and
 653 we fail to utilize the advantage of the Bézier dual basis. Even more, the
 654 sparsity of the constrained stiffness matrix might be impacted as the inverse
 655 of \mathbf{R}_1 is a dense matrix. This type of global factorization has been utilized
 656 for patch coupling problem in [28, 29, 33].

657 Instead of solving the null space directly, we will localize the constraint
 658 to each cross point and solve the null space of a localized linear system. For
 659 the constraint matrix \mathbf{B} constructed by the Lagrange multipliers without
 660 modification, we assume there exist a row permutation matrix $\hat{\mathbf{P}}_r$ such that

$$\hat{\mathbf{B}}_p := \hat{\mathbf{P}}_r \mathbf{B} \tilde{\mathbf{P}}_c^T = \begin{bmatrix} \mathbf{B}_1 \\ \mathbf{B}_2 \end{bmatrix} = \begin{bmatrix} \mathbf{B}_6^1 & \mathbf{B}_6^2 & \mathbf{B}_6^3 & \mathbf{B}_6^4 & \mathbf{B}_6^6 & \mathbf{0} \\ \mathbf{B}_1^1 & \mathbf{B}_1^2 & \mathbf{B}_1^3 & \mathbf{B}_1^4 & \mathbf{B}_1^6 & \mathbf{0} \\ \mathbf{0} & \mathbf{B}_2^2 & \mathbf{B}_2^3 & \mathbf{0} & \mathbf{B}_2^6 & \mathbf{0} \end{bmatrix}, \quad (78)$$

661 with \mathbf{B}_1^1 and \mathbf{B}_2^2 be identity matrices. \mathbf{B}_1 consists of constraints relevant to
 662 cross point while \mathbf{B}_2 consists of constraints relevant to intersections.

663 The null space of \mathbf{B}_2 can be found as

$$\mathbf{C}_2 := \ker(\mathbf{B}_2) = \begin{bmatrix} \mathbf{B}_1^2 \mathbf{B}_2^3 - \mathbf{B}_1^3 & -\mathbf{B}_1^4 & -\mathbf{B}_1^6 & \mathbf{0} \\ -\mathbf{B}_2^3 & \mathbf{0} & -\mathbf{B}_2^6 & \mathbf{0} \\ \mathbf{I} \end{bmatrix}. \quad (79)$$

Due to the inclusion $\hat{\mathbf{C}}_p := \ker(\hat{\mathbf{B}}_p) \subset \ker(\mathbf{B}_2)$, we can construct $\hat{\mathbf{C}}_p$ by

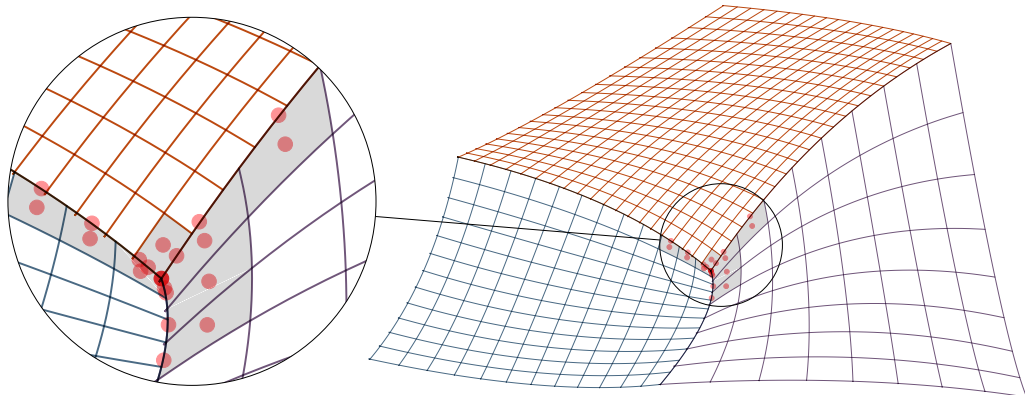


Figure 7: Control points (red) involved in crosspoint constraints (\mathbf{B}_1).

solving $\ker(\mathbf{B}_1 \mathbf{C}_2)$. Since dual basis functions have compact support, \mathbf{B}_1 and

\mathbf{C}_2 are all sparse matrices (control points involved in \mathbf{B}_1 are demonstrated in Figure. 7). We can split the columns of \mathbf{C}_2 into two matrices, as

$$\begin{aligned}\mathbf{C}_2^1 &:= \{v \in \mathbf{C}_2 : \mathbf{B}_1 v \neq 0\}, \\ \mathbf{C}_2^2 &:= \{v \in \mathbf{C}_2 : \mathbf{B}_1 v = 0\}.\end{aligned}\quad (80)$$

Such a split can be defined a priori, based on the discretization of each patch. A demonstration of the split is given in Figure. 8. Note that $\mathbf{C}_2^2 \subset \hat{\mathbf{C}}_p$, $\hat{\mathbf{C}}_p$ can be written as

$$\hat{\mathbf{C}}_p = [\mathbf{C}_2^1 \ker(\bar{\mathbf{B}}_p) \quad \mathbf{C}_2^2], \text{ with } \bar{\mathbf{B}}_p = \mathbf{B}_1 \mathbf{C}_2^1. \quad (81)$$

Compared with the constraint matrix \mathbf{B} whose size increases as we refine

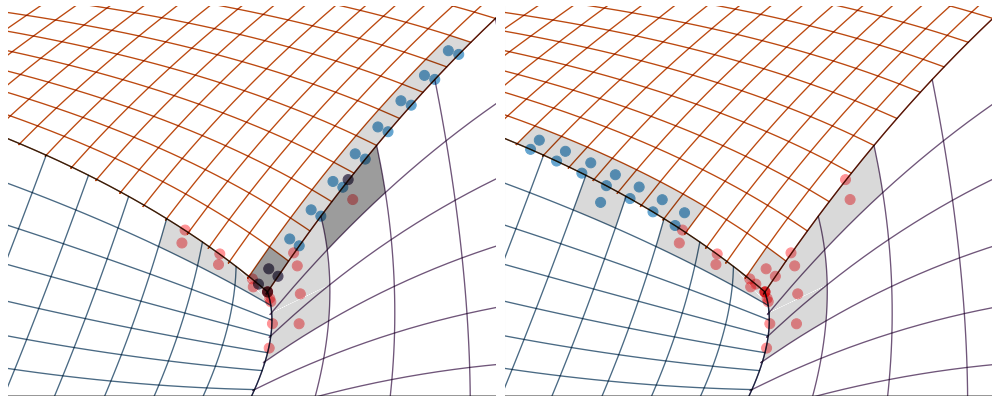


Figure 8: Control points of basis functions (blue) defined by columns of \mathbf{C}_2 . Left: Basis classified to \mathbf{C}_2^1 ; Right: Basis classified to \mathbf{C}_2^2

the mesh, the row size of $\bar{\mathbf{B}}_p$ is fixed and its column size is fixed after certain refinement. A comparison of the size of matrix \mathbf{B} and matrix $\bar{\mathbf{B}}_p$ as a function of the degrees of freedom is given in Figure. 9 for the three-patch coupling in Figure. 5 with 2nd order B-spline basis functions. As can be seen, the size of \mathbf{B} grows rapidly as the mesh being refined. The computational cost of directly solving its kernel will be very expensive. However, owing to the compact support of dual basis function, we can transfer a global, size-varying problem (factorization on \mathbf{B}) to a local, size-fixed problem (factorization on $\bar{\mathbf{B}}_p$), and the problem size is very small (12×24 for this case).

A graphical comparison of the sparsity patterns among standard Lagrange multiplier with global factorization, Bézier dual basis with global factorization and Bézier dual basis with local factorization is given in Figure. 10.

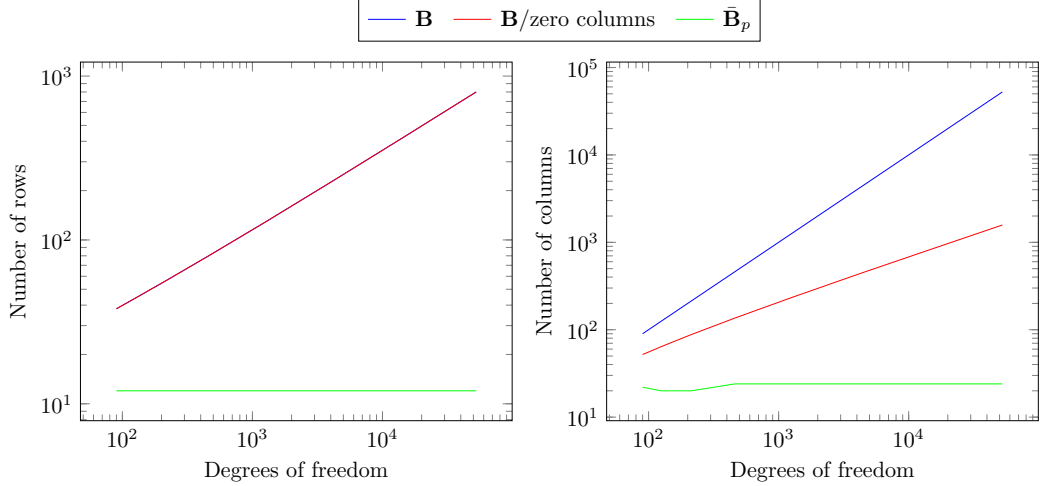


Figure 9: The change of matrix size of \mathbf{B} , \mathbf{B} with zero columns being removed, and $\bar{\mathbf{B}}_p$, as a function of the degrees of freedom. The constraint matrix \mathbf{B} is formulated for the three-patch coupling in Figure. 5 with 2nd order B-spline basis functions.

680 As expected, the standard method yields the lowest sparsity, while Bézier
 681 dual basis with local factorization yields the highest sparsity (40% sparser).
 682 Meanwhile, the Bézier dual basis does not significantly improve the sparsity
 683 if a global factorization is applied to construct \mathcal{K}_b^h . Moreover, a global fac-
 684 torization yeilds entries with very small absolute values ($\leq 10^{-14}$), especially
 685 for the constraint matrix formed by Bézier dual basis, while all entries are
 686 away from zero for the local factorization.

687 7. Numerical results for biharmonic problems

688 All our numerical results are obtained via an in-house C++ code.

689 7.1. A numerical study of the completeness of Bézier dual basis

690 We consider the completeness of Bézier dual basis on the one dimensional
 691 domain, $\Omega = (0, 1)$. The domain Ω is uniformly partitioned into two elements,
 692 since the Bézier dual basis is equivalent to the global dual basis on one
 693 element domain. In the numerical test, we find the L^2 approximation of n^{th}
 694 order Legendre polynomial in the Bézier dual space, as Legendre polynomials
 695 are orthogonal to each other.

696 The test results are disappointed, the Bézier dual basis of arbitrary order
 697 is only complete for zeroth order polynomial i.e., only the error of the L^2

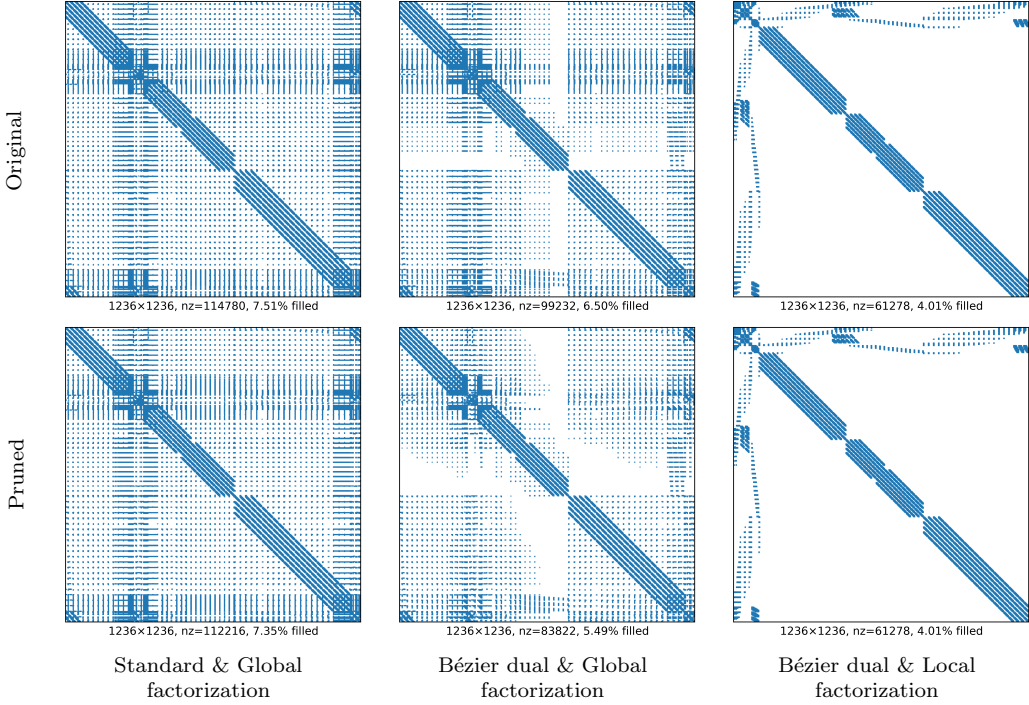


Figure 10: Sparsity patterns of constrained stiffness matrices. Left: standard Lagrange multipliers with global factorization. Middle: Bézier dual basis with global factorization. Right: Bézier dual basis with localized factorization. Top: original matrix. Bottom: small absolute values ($\leq 10^{-14}$) be pruned. All stiffness matrices are formulated for the three-patch coupling in Figure 5 with 3rd order B-spline basis functions after 4 refinements. The number of non-zero entries is given by nz.

698 projection of constant function is below the round-off error. The results of
 699 projecting Legendre polynomials up to 3rd order onto 3rd order Bézier dual
 700 basis are demonstrated in Fig. 11. As can be seen, there are huge discrep-
 701 ancies between the approximations and original functions for all Legendre
 702 polynomials except constant. In other words, the L^2 approximation of Bézier
 703 dual basis is only of first-order, which might deteriorate the optimality of the
 704 finite element approximation.

705 In the finite element context, the construction of dual basis that can
 706 reproduce polynomial of degree $p - 1$ is thoroughly studied in [71]. However,
 707 the construction procedure is complicated and gets even worse for higher
 708 inter-element continuity. Following this approach, a $p - 1$ complete dual
 709 basis function for a quadratic B-spline basis function was constructed in [22],

710 but its support is much larger than its B-spline counterpart. On the other
 711 side, though the poor polynomial completeness, Bézier dual basis can be
 712 constructed in a straightforward manner, without solving additional linear
 713 system. Hence, in the rest examples, we will testify the performance of C^1
 714 dual mortaring and the influence of the Bézier dual basis on the optimality
 715 of the finite element approximation.

716 *7.2. Biharmonic problem on a two-patch domain*

717 We first solve a biharmonic problem $\Delta^2 u = f$ on a square domain $\Omega =$
 718 $(0, 1) \times (0, 1)$. The manufactrued solution is given as

$$u(x, y) = \sin(2\pi x) \sin(2\pi y) (xy(x - 1)(y - 1))^2, \quad (82)$$

719 which satisfies the homogeneous Dirichlet boundary condition ($u = \frac{\partial u}{\partial n} =$
 720 0) and is visualized in Figure. 12. The domain Ω is decomposed into two
 721 patches, namely $\Omega_1 = (0, 0.4) \times (0, 1)$ and $\Omega_2 = (0.4, 1) \times (0, 1)$, as shown in
 722 Figure. 12a. The right-hand side function f can be obtained by applying the
 723 biharmonic operator to u .

724 We conduct convergence studies for $p = 2, 3, 4, 5$ in both L^2 norm and
 725 H^2 norm, as shown in Fig. 13. However, though the theoretical flaw of
 726 Bézier dual basis, its performances in real problem are surprisingly well. As
 727 can be seen, both global dual basis and Bézier dual basis obtain optimal
 728 convergence rate in both norm measures for all polynomial degrees (The op-
 729 timal convergence rate for $p = 2$ in L^2 norm is 2, which can be testified by
 730 Aubin-Nitsche duality argument[][],). One conjecture can be made is that
 731 for biharmonic problems, the coefficients of the best approximation error of
 732 Lagrange multipliers are very small so that their contribution in the finite el-
 733 ement approximation error can be ignored. Moreover, the accuracy of Bézier
 734 dual basis are higher than that of global dual basis with the same refinement
 735 level.

736 To study the performance of proposed methods in detail, we consider ex-
 737 treme conditions e.g. distorted mesh (Figure. 12b), mismatched mesh (Fig-
 738 ure. 12c) and mismatched degree ($p_1 = p_2 + 1$), respectively. For the distorted
 739 mesh, the proposed method with both global dual basis and Bézier dual ba-
 740 sis perform similarly, the optimal convergence rates are reached for all cases.
 741 Some superconvergence behavior are observed (e.g. $p = 3$ for both global and
 742 Bézier dual basis). This partially due to the geometrical locking existed in
 743 deformed meshes. For the mismatched mesh, the convergence performance

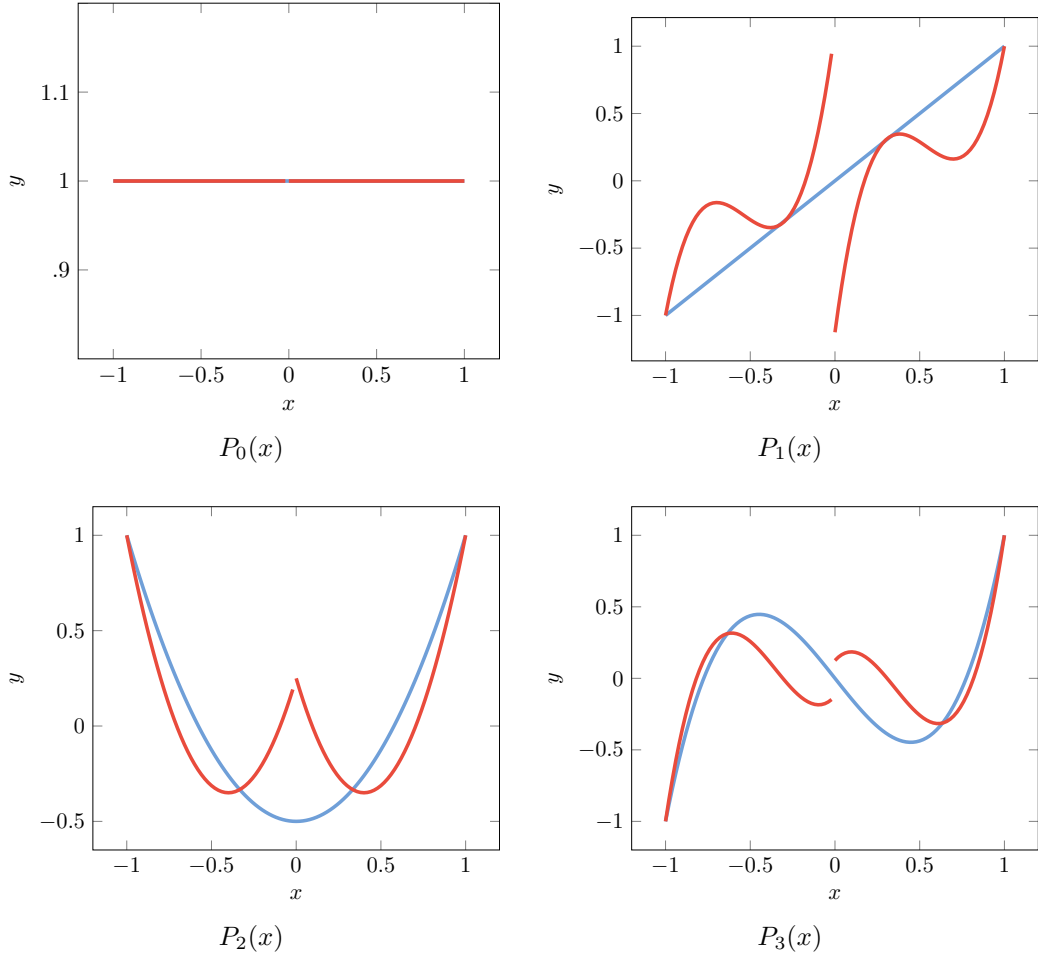


Figure 11: The Legendre polynomials (—) and their approximations (—) in 3^{rd} order Bézier dual space composed of two elements. Bézier dual basis cannot duplicate all except the constant function.

744 of Bézier dual basis, though remains optimality, suffers a vertical lift of the
 745 error curves, which indicates that the Bézier dual basis are more sensitive to
 746 the mesh quality. However, for the finer mesh, the result obtained by 5th
 747 order global dual basis become sub-optimal, we speculate this is caused by the
 748 *inf-sup* instability in this specific circumstance. For the degree mismatched
 749 case, as expected, the convergence rates are between $p + 1$ and $p + 2$ in L^2
 750 norm, and between $p - 1$ and p in H^2 norm for all tested cases.

751 Although a functional analysis of the contributions of the Lagrange multipliers' best approximation error in the finite element approximation error is
 752 beyond the scope of this paper and postponed to future work, here we study
 753 their influence in a numerical manner. The best approximation of u in the
 754 discretized weak C^1 space \mathcal{K}_b^h can be given as: find $u \in \mathcal{K}_b^h$ such that

$$\langle v^h, u^h \rangle_{H^2} = \langle v^h, u \rangle_{H^2} \quad \forall v^h \in \mathcal{K}_b^h. \quad (83)$$

755 The best H^2 approximation error for the proposed methods for all scenarios are shown in Fig. 17. As can be seen, the convergence plots of the best
 756 H^2 approximation error are identical to that of the finite element approximation error in H^2 norm. The best H^2 approximation errors for all cases are
 757 no more than 1% smaller than that of the finite element counterparts, which
 758 confirms our speculation that the contribution of the Lagrange multipliers' best approximation errors are negligible for tested problems. In addition, the
 759 best approximation error for the $p = 5$ global dual basis in the mismatched
 760 non-conforming mesh test case also suffers rate decrease, which confirms that
 761 the main cause of the rate slow down is due to the *inf-sup* instability.

766 7.3. Biharmonic problem on multi-patch domains

767 Let us now exam the effect of the presence of cross-points. We first solve
 768 a biharmonic problem with the manufactured solution

$$u(x, y) = \sin(2\pi x)\sin(2\pi y) (y(3x - y)(3x + 2y - 9))^2, \quad (84)$$

769 on a triangular domain decomposed into three patches, as shown in
 770 Fig. 18.

771 The convergence behaviors of the proposed methods are studied in Fig. 19.
 772 For polynomial order $p = 2, 3, 4$, the convergence results of both global dual
 773 and Bézier dual in L^2 and H^2 norm are in accordance with the finite element
 774 approximation theory. However, for $p = 5$, sub-optimality are observed for

775 both methods in both norm measures in the 5th refinement. The H^2 pro-
 776 jection convergence plot reveals that the causes of the rate slow down for
 777 global dual and Bézier dual are different. For Bézier dual, the H^2 projec-
 778 tion errors decay theoretically, which indicates that the rate slow down in
 779 corresponding biharmonic problem is due to the poor approximation of the
 780 Bézier dual basis. The rate slow down is also observed in the H^2 projection of
 781 global dual case, which means the main cause of the rate slow down of global
 782 dual case is the *inf-sup* instability. Nonetheless, despite this sub-optimal
 783 convergence, the proposed methods still converge asymptotically.

784 Whereas the poor polynomial completeness of Bézier dual basis does not
 785 affect the performance of two patch coupling, we do observe its influence
 786 for multi-patch coupling with the presence of the cross-point. To further
 787 demonstrate the effect of the presence of cross-points, we solve a biharmonic
 788 problem on a five-patch domain, with the analytical solution

$$u(x, y) = \sin(2\pi x)^2 \sin(2\pi y)^2, \quad (85)$$

789 as shown in Fig. 20. The convergence behaviors, demonstrated in Fig. 21, are
 790 similar to that of the three-patch case. The introducing of more cross-points
 791 and more coupled intersections seems does not deteriorate the performances
 792 of the proposed methods. Without constructing a dual basis with higher
 793 order polynomial completeness, a feasible way to recover the optimality of
 794 the coupling algorithm is to locally refine the basis function on the slave
 795 side [95]. Though the tensor product structures of each patches are lost, no
 796 additional degrees of freedom are introduced to the constrained problem and
 797 the domination of Lagrange multiplier approximation error can be postponed.

798 8. Schedule

799 Although there are various aspects in weak C^1/G^1 coupling deserve a
 800 thorough study, our main focus in this stage is to extend our finding in an ab-
 801 stract problem (biharmonic problem) to practical problems (e.g. Kirchhoff-
 802 Love shell). Compared to the planar biharmonic problem, Kirchhoff-Love
 803 shell is a more challenging problem, as the computational domain is in \mathbb{R}^3
 804 and the constraint is not isotropically applied in each direction. Hence, a
 805 more generalized constraint is needed to compromise geometries with kinks.
 806 And validations are needed for two-patch and multi-patch Kirchhoff-Love
 807 shells. Meanwhile, although we have implemented two algorithms to solve

808 multi-patch biharmonic problems, the boundary modification method does
 809 not deliver ideal results while an additional factorization is needed for ex-
 810 plicitly solving the null space. We will still make efforts in finding a feasi-
 811 ble boundary modification for multi-patch coupling. A detailed time line is
 812 shown in Table. 2.

813 **9. Weak coupling for Kirchhoff-Love shell**

814 *9.1. Kirchhoff-Love shell formulation*

815 A thin shell is defined as a shell with a thickness which is small compared
 816 to its other dimensions. Hence, the geometry description of a thin shell can
 817 be given by its middle surface and the corresponding thickness. Here, we use
 818 $\mathbf{X}(\xi, \eta), \mathbf{x}(\xi, \eta) : \mathbb{R}^2 \rightarrow \mathbb{R}^3$ to describe the middle surface of a shell in the
 819 reference and current configurations, respectively. The middle surface base
 820 vectors in both configurations are defined as

$$\begin{cases} \mathbf{A}_1 = \frac{\partial \mathbf{X}}{\partial \xi} \\ \mathbf{A}_2 = \frac{\partial \mathbf{X}}{\partial \eta} \\ \mathbf{A}_3 = \frac{\mathbf{A}_1 \times \mathbf{A}_2}{|\mathbf{A}_1 \times \mathbf{A}_2|} \end{cases}, \quad \begin{cases} \mathbf{a}_1 = \frac{\partial \mathbf{x}}{\partial \xi} \\ \mathbf{a}_2 = \frac{\partial \mathbf{x}}{\partial \eta} \\ \mathbf{a}_3 = \frac{\mathbf{a}_1 \times \mathbf{a}_2}{|\mathbf{a}_1 \times \mathbf{a}_2|} \end{cases}. \quad (86)$$

821 The covariant and contravariant components of the surface metric tensors in
 822 both configurations are:

$$A_{ij} = \mathbf{A}_i \cdot \mathbf{A}_j, \quad a_{ij} = \mathbf{a}_i \cdot \mathbf{a}_j, \quad A^{ij} = A_{ij}^{-1}, \quad a^{ij} = a_{ij}^{-1}. \quad (87)$$

The reference \mathbf{R} and current \mathbf{r} position vectors of a material point on a thin
 shell can be parameterized as

$$\mathbf{R} = \mathbf{X}(\xi, \eta) + \zeta \mathbf{A}_3(\xi, \eta), \quad (88)$$

$$\mathbf{r} = \mathbf{x}(\xi, \eta) + \zeta \mathbf{a}_3(\xi, \eta), \quad \zeta \in \left[-\frac{h}{2}, \frac{h}{2} \right]. \quad (89)$$

823 The displacement vector of the middle surface is defined as

$$\mathbf{u}(\xi, \eta) = \mathbf{x}(\xi, \eta) - \mathbf{X}(\xi, \eta). \quad (90)$$

824 The covariant base vectors in both configurations are

$$\begin{cases} \mathbf{G}_1 = \frac{\partial \mathbf{R}}{\partial \xi} \\ \mathbf{G}_2 = \frac{\partial \mathbf{R}}{\partial \eta} \\ \mathbf{G}_3 = \frac{\mathbf{G}_1 \times \mathbf{G}_2}{|\mathbf{G}_1 \times \mathbf{G}_2|} \end{cases}, \quad \begin{cases} \mathbf{g}_1 = \frac{\partial \mathbf{r}}{\partial \xi} \\ \mathbf{g}_2 = \frac{\partial \mathbf{r}}{\partial \eta} \\ \mathbf{g}_3 = \frac{\mathbf{g}_1 \times \mathbf{g}_2}{|\mathbf{g}_1 \times \mathbf{g}_2|} \end{cases}. \quad (91)$$

⁸²⁵ The covariant metric coefficients in both configurations are defined as

$$G_{ij} = \mathbf{G}_i \cdot \mathbf{G}_j, \quad g_{ij} = \mathbf{g}_i \cdot \mathbf{g}_j. \quad (92)$$

⁸²⁶ The contravariant base vectors are computed by

$$\mathbf{G}^i = G^{ij} \mathbf{G}_j, \quad \mathbf{g}^i = g^{ij} \mathbf{g}_j, \quad (93)$$

⁸²⁷ with

$$g^{ij} = g_{ij}^{-1}, \quad G^{ij} = G_{ij}^{-1}. \quad (94)$$

⁸²⁸ The Green-Lagrange strain tensor is

$$\mathbf{E} = \frac{1}{2} (\mathbf{F}^T \mathbf{F} - \mathbf{I}). \quad (95)$$

⁸²⁹ With

$$\mathbf{F} = \mathbf{g}_i \otimes \mathbf{G}^i, \quad (96)$$

⁸³⁰ equation (95) can be rewritten as

$$\mathbf{E} = E_{ij} \mathbf{G}^i \otimes \mathbf{G}^j = \frac{1}{2} (g_{ij} - G_{ij}) \mathbf{G}^i \otimes \mathbf{G}^j. \quad (97)$$

Under the assumption that straight lines normal to the mid-surface remain straight and normal to the mid-surface after deformation, the transverse shear strains of a Kirchhoff-Love shell vanish ($E_{\alpha 3} = 0$). The strains can be split into membrane strains and bending strains [15]:

$$E_{\alpha\beta} = \epsilon_{\alpha\beta} + \zeta \kappa_{\alpha\beta}, \quad (98)$$

$$\epsilon_{\alpha\beta} = \frac{1}{2} (a_{\alpha\beta} - A_{\alpha\beta}), \quad (99)$$

$$\kappa_{\alpha\beta} = \mathbf{a}_3 \cdot \mathbf{a}_{\alpha,\beta} - \mathbf{A}_3 \cdot \mathbf{A}_{\alpha,\beta}. \quad (100)$$

The corresponding membrane and bending stresses are given as:

$$n^{\alpha\beta} = \frac{Eh}{1-\nu^2} H^{\alpha\beta\gamma\delta} \epsilon_{\gamma\delta}, \quad (101)$$

$$m^{\alpha\beta} = \frac{Eh^3}{12(1-\nu^2)} H^{\alpha\beta\gamma\delta} \kappa_{\gamma\delta}, \quad (102)$$

⁸³¹ where E is the Young's modulus, ν is Poisson's ratio, and

$$H^{\alpha\beta\gamma\delta} = \nu A^{\alpha\beta} A^{\gamma\delta} + \frac{1}{2}(1-\nu) (A^{\alpha\gamma} A^{\beta\delta} + A^{\alpha\delta} A^{\beta\gamma}). \quad (103)$$

To restrict the analysis to small deformation, the membrane strains and bending strains are linearized as

$$\epsilon_{\alpha\beta} = \frac{1}{2} (\mathbf{A}_\alpha \cdot \mathbf{u}_{,\beta} + \mathbf{u}_{,\alpha} \cdot \mathbf{A}_\beta), \quad (104)$$

$$\begin{aligned} \kappa_{\alpha\beta} &= -\mathbf{u}_{,\alpha\beta} \cdot \mathbf{A}_3 + \frac{1}{\sqrt{|\mathbf{A}_1 \times \mathbf{A}_2|}} (\mathbf{u}_{,1} \cdot (\mathbf{A}_{\alpha,\beta} \times \mathbf{A}_2) + \mathbf{u}_{,2} \cdot (\mathbf{A}_1 \times \mathbf{A}_{\alpha,\beta})) \\ &\quad + \frac{\mathbf{A}_3 \cdot \mathbf{A}_{\alpha,\beta}}{\sqrt{|\mathbf{A}_1 \times \mathbf{A}_2|}} (\mathbf{u}_{,1} \cdot (\mathbf{A}_2 \times \mathbf{A}_3) + \mathbf{u}_{,2} \cdot (\mathbf{A}_3 \times \mathbf{A}_1)). \end{aligned} \quad (105)$$

832 need to add equilibrium..

833 *9.2. Continuity constraints*

834 For the multi-patch formulation of the Kirchhoff-Love shell, the C^0 con-
835 tinuity must be satisfied by the displacement field \mathbf{u} so that the deformed
836 geometry remains continuous. However, in the linearized bending strain $\kappa_{\alpha\beta}$,
837 the second order derivative $\mathbf{u}_{,\alpha\beta}$ appears, and therefore an additional con-
838 straint is required. From the physical perspective, the additional constraint
839 should deliver the bending moment from one patch to another; from the
840 mathematical perspective, the additional constraint should ensure the lin-
841 earized bending strain $\kappa_{\alpha\beta}$ to be square integrable.

842 For a smooth Kirchhoff-Love shell, *i.e.* the director \mathbf{A}_3 is continuous, $\kappa_{\alpha\beta}$
843 is square integrable if \mathbf{u} is C^1 continuous. However, shell structures are not
844 necessarily smooth, geometries with kinks and folds are commonly used in
845 engineering practices. Hence, a generalized constraint should be developed
846 to handle these non-trivial patch configurations.

A Kirchhoff-Love shell with the appearance of kinks is demonstrated in Fig. 22, where the intersection between the slave patch Ω_s and the master patch Ω_m is denoted by the red curve. The kink appears as the director \mathbf{A}_3^s and \mathbf{A}_3^m are not the same. A rotation tensor \mathbf{R} from \mathbf{A}_3^s to \mathbf{A}_3^m can be determined by the Rodrigues's rotation formula as:

$$\mathbf{v} = \mathbf{A}_3^s \times \mathbf{A}_3^m, \quad (106)$$

$$c = \mathbf{A}_3^s \cdot \mathbf{A}_3^m, \quad (107)$$

$$\mathbf{R} = \mathbf{I} + [\mathbf{v}]_\times + \frac{1}{1+c} [\mathbf{v}]_\times^2, \quad (108)$$

⁸⁴⁷ where $[\bullet]_{\times}$ is the skew-symmetric matrix form of the cross product $\bullet \times$,

$$[\mathbf{v}]_{\times} = \begin{bmatrix} 0 & -v_3 & v_2 \\ v_3 & 0 & -v_1 \\ -v_2 & v_1 & 0 \end{bmatrix}. \quad (109)$$

Similar to the biharmonic problem, we extend the local coordinate system (ξ_s, η_s) of Ω_s to Ω_m , such that

$$\mathbf{A}_1^{m'}: = \frac{\partial \mathbf{X}_m}{\partial \xi_s} = \mathbf{R} \mathbf{A}_1^s, \quad (110)$$

$$\mathbf{A}_2^{m'}: = \frac{\partial \mathbf{X}_m}{\partial \eta_s} = \mathbf{R} \mathbf{A}_2^s. \quad (111)$$

⁸⁴⁸ The Jacobian matrix

$$\mathbf{J} := \begin{bmatrix} \frac{\partial \xi_m}{\partial \xi_s} & \frac{\partial \xi_m}{\partial \eta_s} \\ \frac{\partial \eta_m}{\partial \xi_s} & \frac{\partial \eta_m}{\partial \eta_s} \end{bmatrix}, \quad (112)$$

⁸⁴⁹ can be obtained by solving the following linear problem

$$\left[\frac{\partial \mathbf{X}_m}{\partial \xi_m} \quad \frac{\partial \mathbf{X}_m}{\partial \eta_m} \right] \cdot \mathbf{J} = [\mathbf{R} \mathbf{A}_1^s \quad \mathbf{R} \mathbf{A}_2^s]. \quad (113)$$

⁸⁵⁰ The derivatives of \mathbf{u}_m w.r.t. directions $\mathbf{A}_1^{m'}$ and $\mathbf{A}_2^{m'}$ can be found as

$$\left[\frac{\partial \mathbf{u}_m}{\partial \mathbf{A}_1^{m'}} \quad \frac{\partial \mathbf{u}_m}{\partial \mathbf{A}_2^{m'}} \right] := \left[\frac{\partial \mathbf{u}_m}{\partial \xi_s} \quad \frac{\partial \mathbf{u}_m}{\partial \eta_s} \right] = \left[\frac{\partial \mathbf{u}_m}{\partial \xi_m} \quad \frac{\partial \mathbf{u}_m}{\partial \eta_m} \right] \cdot \mathbf{J}. \quad (114)$$

⁸⁵¹ Now, let us consider the square integrability of the first term of equation (105). The restriction of this term on the slave patch and the master patch are:

$$\mathbf{u}_{,\alpha\beta} \cdot \mathbf{A}_3|_{\Omega_s} = \frac{\partial^2 \mathbf{u}_s}{\partial \mathbf{A}_\alpha^s \partial \mathbf{A}_\beta^s} \cdot \mathbf{A}_3^s, \quad (115)$$

⁸⁵⁴ and

$$\begin{aligned} \mathbf{u}_{,\alpha\beta} \cdot \mathbf{A}_3|_{\Omega_m} &= \frac{\partial^2 \mathbf{u}_m}{\partial \mathbf{A}_\alpha^{m'} \partial \mathbf{A}_\beta^{m'}} \cdot \mathbf{A}_3^m \\ &= \frac{\partial^2 \mathbf{u}_m}{\partial \mathbf{A}_\alpha^{m'} \partial \mathbf{A}_\beta^{m'}} \cdot \mathbf{R} \mathbf{A}_3^s \\ &= \mathbf{R}^T \frac{\partial^2 \mathbf{u}_m}{\partial \mathbf{A}_\alpha^{m'} \partial \mathbf{A}_\beta^{m'}} \cdot \mathbf{A}_3^s \\ &= \frac{\partial^2 \mathbf{R}^T \mathbf{u}_m}{\partial \mathbf{A}_\alpha^s \partial \mathbf{A}_\beta^s} \cdot \mathbf{A}_3^s. \end{aligned} \quad (116)$$

Hence, the bending strains are square integrable if \mathbf{u}_s and $\mathbf{R}^T \mathbf{u}_m$ is C^1 continuous across the intersection:

$$\begin{cases} \frac{\partial \mathbf{u}_s}{\partial \mathbf{A}_1^s} = \mathbf{R}^T \frac{\partial \mathbf{u}_m}{\partial \mathbf{A}_1^{m'}} \\ \frac{\partial \mathbf{u}_s}{\partial \mathbf{A}_2^s} = \mathbf{R}^T \frac{\partial \mathbf{u}_m}{\partial \mathbf{A}_2^{m'}} \end{cases}, \quad \text{or} \quad \begin{cases} \frac{\partial \mathbf{u}_s}{\partial \xi_s} = \mathbf{R}^T \frac{\partial \mathbf{u}_m}{\partial \xi_s} \\ \frac{\partial \mathbf{u}_s}{\partial \eta_s} = \mathbf{R}^T \frac{\partial \mathbf{u}_m}{\partial \eta_s} \end{cases}. \quad (117)$$

855 *Remark 1.* Note that in the cases of smooth shell couplings, \mathbf{R} is an identity
856 tensor and $\mathbf{A}_1^{m'} = \mathbf{A}_1^s$, $\mathbf{A}_2^{m'} = \mathbf{A}_2^s$, the constraints (117) reduce to the C^1
857 continuity of \mathbf{u}_s and \mathbf{u}_m .

858 *Remark 2.* Under the constraints (117), the angle of the kink is preserved in
859 the current configuration, that is: if $\mathbf{A}_3^m = \mathbf{R}\mathbf{A}_3^s$, then we have $\mathbf{a}_3^m = \mathbf{R}\mathbf{a}_3^s$.

860 To show this, we first linearize the normal directors in the current con-
861 figuration of the slave patch as:

$$\mathbf{a}_3^s = \mathbf{A}_3^s + \frac{\frac{\partial \mathbf{u}_s}{\partial \xi_s} \times \mathbf{A}_2^s + \mathbf{A}_1^s \times \frac{\partial \mathbf{u}_s}{\partial \eta_s} - \mathbf{A}_3^s \left(\left(\frac{\partial \mathbf{u}_s}{\partial \xi_s} \times \mathbf{A}_2^s + \mathbf{A}_1^s \times \frac{\partial \mathbf{u}_s}{\partial \eta_s} \right) \cdot \mathbf{A}_3^s \right)}{|\mathbf{A}_1^s \times \mathbf{A}_2^s|}, \quad (118)$$

862 after applying the rotation tensor and using the fact that, for a rotation
863 tensor \mathbf{R} , $\mathbf{R}(\mathbf{a} \times \mathbf{b}) = \mathbf{R}\mathbf{a} \times \mathbf{R}\mathbf{b}$, we obtain:

$$\begin{aligned} \mathbf{R}\mathbf{a}_3^s &= \mathbf{A}_3^m + \frac{\frac{\partial \mathbf{u}_m}{\partial \xi_s} \times \mathbf{A}_2^m + \mathbf{A}_1^m \times \frac{\partial \mathbf{u}_m}{\partial \eta_s} - \mathbf{A}_3^m \left(\left(\frac{\partial \mathbf{u}_m}{\partial \xi_s} \times \mathbf{A}_2^m + \mathbf{A}_1^m \times \frac{\partial \mathbf{u}_m}{\partial \eta_s} \right) \cdot \mathbf{A}_3^m \right)}{|\mathbf{A}_1^m \times \mathbf{A}_2^m|} \\ &= \mathbf{a}_3^m. \end{aligned} \quad (119)$$

864 Indeed, the preserving of rotation angle between kink provides a physical
865 evidence of the correctness of the constraints (117).

866 9.3. Dual mortaring formulation for Kirchhoff-Love shell

867 Under the body force \mathbf{q} and the traction \mathbf{t} , the weak form of the shell can
868 be formulated by the equilibrium of virtual work as: find $\mathbf{u} \in \mathcal{K}_b^{kl}$, such that

$$\int_{\Omega} (n^{\alpha\beta}(\mathbf{u})\delta\epsilon_{\alpha\beta}(\mathbf{v}) + m^{\alpha\beta}(\mathbf{u})\delta\kappa_{\alpha\beta}(\mathbf{v})) d\Omega = \int_{\Omega} \mathbf{q} \cdot \mathbf{v} d\Omega + \int_{\Gamma} \mathbf{t} \cdot \mathbf{v} d\Gamma, \quad \forall \mathbf{v} \in \mathcal{K}_b^{kl}. \quad (120)$$

869 The constrained function space \mathcal{K}_b^{kl} is

$$\mathcal{K}_b^{kl} := \left\{ \mathbf{u} \in [\mathcal{X}_b]^3 : b_0^{kl}(\mathbf{u}, \boldsymbol{\mu}_0) = 0 \text{ and } b_1^{kl}(\mathbf{u}, \boldsymbol{\mu}_1) = 0 \quad \forall (\boldsymbol{\mu}_0, \boldsymbol{\mu}_1) \in [\mathcal{M}_0]^3 \times [\mathcal{M}_1]^3 \right\}, \quad (121)$$

where

$$b_0^{kl}(\mathbf{u}, \boldsymbol{\mu}) = \int_{\Gamma_{sm}} \boldsymbol{\mu} \cdot [\mathbf{u}]_\Gamma d\Gamma, \quad (122)$$

$$b_1^{kl}(\mathbf{u}, \boldsymbol{\mu}) = \int_{\Gamma_{sm}} \boldsymbol{\mu} \cdot \left(\frac{\partial \mathbf{u}_s}{\partial \xi_s} - \mathbf{R}^T \frac{\partial \mathbf{u}_m}{\partial \xi_s} \right) d\Gamma. \quad (123)$$

870 The discretizations of $[\mathcal{X}_b]^3$, $[\mathcal{M}_0]^3$ and $[\mathcal{M}_1]^3$ are identical to the biharmonic problem, and a similar approach can be applied to treat the cross point problem for the multi-patch Kirchhoff-Love shell coupling.

873 *Remark 3.* This manuscript is not the first one that discussing the multi-patch coupling of Kirchhoff-Love shell problem in the IGA framework. Compared to published methods, the proposed procedure is advance in that:

- 876 • Whereas the bending strip method [58] requires C^0 continuity and en-
877 forces constraints by penalty method, the proposed method can be
878 applied to arbitrary discretizations and constraints are applied accu-
879 rately.
- 880 • Whereas the Coox's collocation method [29] solves the nullspace of a
881 global constraint matrix resulting in a densed global stiffness matrix,
882 the proposed constraints are dual basis friendly and the sparsity of the
883 constrained linear system is preserved.
- 884 • Whereas the Nitsche's method (e.g. [45]) requires the constructions of
885 additional terms, whose formulations vary with respect to the consti-
886 tutive equations, the proposed method only depend on the geometry
887 and is independent of the choice of material model. In addition, the
888 stiff matrix size of the proposed method is smaller than that of the
889 Nitsche's method of the same degrees of freedom.

890 **10. Numerical examples for Kirchhoff-Love shell problems**

891 *10.1. Scordelis-Lo roof*

892 We first consider the Scordelis-Lo roof benchmark problem. The Scordelis-
893 Lo roof problem is a membrane stress dominated static shell problem and

894 named after the authors who first reported it [77]. In this problem, a cylindrical shell roof (Young's modulus $E = 432\text{MPa}$, Poisson's ratio $\nu = 0$, thickness $t = 0.25\text{m}.$), under the distributed gravity load ($f = 90\text{N/m}^2$), is supported by rigid diaphragms on both curved edges (i.e. $u_x = u_z = 0$), while the straight edges are free to move, as depicted in Figure. 23a. To improve the robustness, the displacement in y direction of one DOF on the diaphragms supported edges is fixed. The vertical displacement at the mid-point of the straight edges is considered as the reference (with the given value $u_z = -0.300592457\text{m}$).

903 The roof structure is decomposed into four patches, which are discretized
904 non-conformally as shown in Fig. 23b. Fig. 24 shows the convergent behaviors
905 of the global dual and the Bézier dual for different polynomial degrees.
906 Converged results are obtained for all polynomial orders. For quartic basis
907 functions, the relative error is reduced to 0.1% with only one refinement for
908 both methods. The convergence performance of the Bézier dual is better
909 than that of the global dual for quadratic and cubic cases. Although the
910 Bézier dual yeilds slightly higher error for the quartic case, it still converges
911 asymptotically.

912 Fig. 25 demonstrates the effect of the proposed constraint. As can be seen,
913 with only C^0 continuity constraint enforced, althought the deformed surface
914 remains continuous, the intersections fail to pass the bending moments from
915 one patch to another. Hence, kinks are formed along all intersections. By
916 enforcing the additional constraint, the smoothness of the roof structure is
917 preserved, even though the mesh is non-conformly discretized.

918 10.2. L-shaped cantilever beam

919 In this section, we consider shell patches meet at angles other than 0° to
920 see how the proposed method handles shell geometries with kinks.

921 We first take a two patch L-shaped beam, where patches are joined at
922 90° . The geometry information and boundary conditions are demonstrated in
923 Fig. 26a. The two patches have the same thickness of $t = 0.2$. The material
924 properties for both patches are: Young's modulus $E = 3 \times 10^6$, Poisson's
925 ratio $\nu = 0.3$. A point load of $F = 10$ is applied at the top left corner of the
926 top flange. The L-shaped cantilever beam is discretized non-comformly, as
927 depicted in Fig. 26b.

928 We consider the vertical displacement of the tip under loading, and compare
929 the obtained results with a converged shell element result from Abaqus,
930 see Fig. 27. The converged solution for both dual basis functions is $u_z =$

931 -0.03835 , which is slightly higher than the reference value $u_z = -0.03913$
932 obtained from Abaqus. Fig. 28a shows the deformed beam with only C^0
933 continuity constraint. For this case, the hinge serves like a hinge between
934 patches and no bending moment is transferred. The proposed constraint is
935 applied in Fig. 28b, where the 90° angle is preserved during the deformation,
936 which is consistent with Remark. 2.

937 We next quantitatively study the performance of the proposed constraint
938 in preserving angle between coupled patches. Beside the L-shaped beam with
939 a constant angle of 90° between two patches, a generalized L-shaped beam
940 with variant angles is also considered, cf. Fig. 29. The loading, boundary
941 conditions and material properties remain the same as the previous example.
942 Both patches are discretized by bicubic elements and two h -refinements are
943 conducted in each directions. The relative errors of the coupling angle along
944 the interface for both cases are shown in Fig. 30. For the case of the constant
945 coupling angle, the maximum relative errors along the intersection are only
946 7×10^{-7} for both global dual and Bézier dual basis functions. A similar test
947 has been conducted for a T-beam coupled by a Nitsche type method [45],
948 where a larger maximum relative error of 2×10^{-6} is obtained for a deforma-
949 tion magnitude that is ten times smaller than that of this benchmark. For
950 the case of variant coupling angles, the relative errors are still acceptable,
951 though they are slightly larger than the previous case. For both cases, the
952 maximum relatives errors are obtained at the furthest position from the fixed
953 boundary, where the highest deformation happens. This is consistent with
954 the fact that the angle preservation property of the proposed constraint is
955 verified under the small deformation assumption.

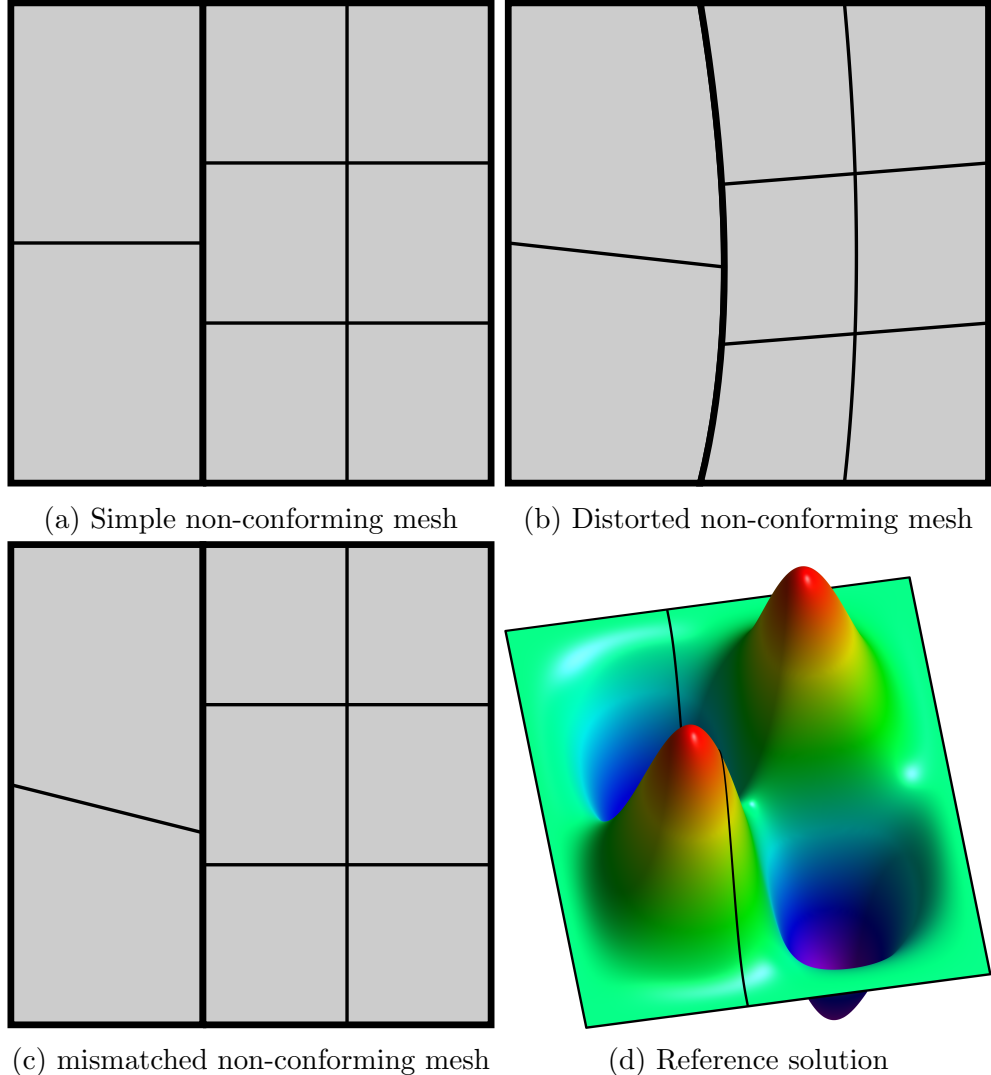


Figure 12: The discretizations of computational domain Ω and the manufactured solution with the property $u = \frac{\partial u}{\partial \mathbf{n}} = 0$ on $\partial\Omega$, which are used in Section 7.2.

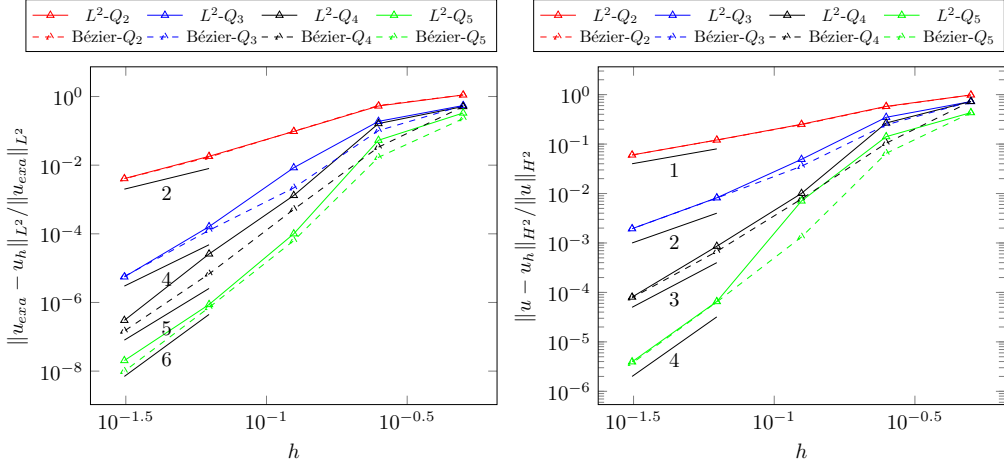


Figure 13: Convergence plot for simple non-conforming patch coupling in 7.2. Left: error measured in L^2 norm. Right: error measured in H^2 norm.

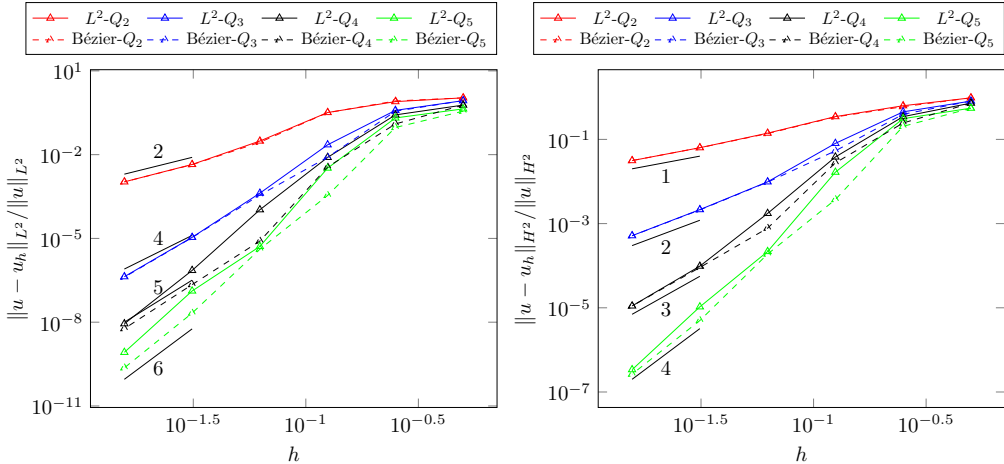


Figure 14: Convergence plot for distorted non-conforming patch coupling in 7.2. Left: error measured in L^2 norm. Right: error measured in H^2 norm.

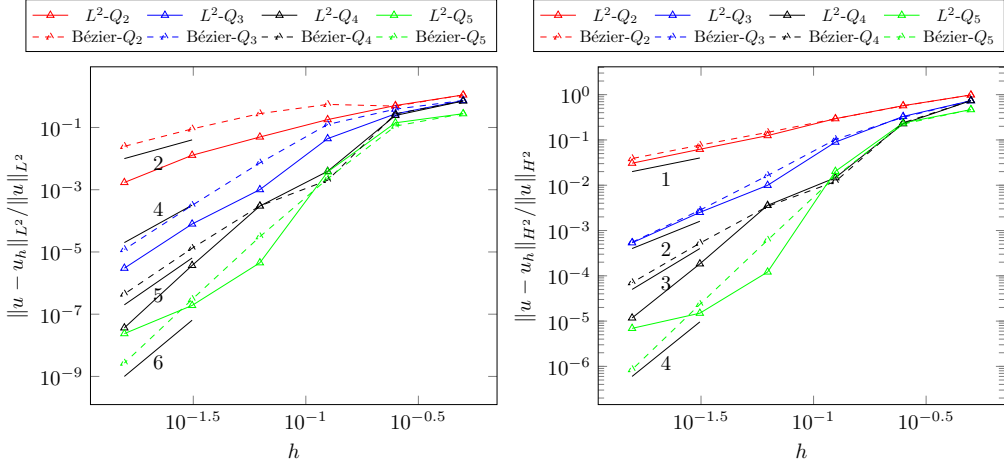


Figure 15: Convergence plot for mesh mismatched non-conforming patch coupling in 7.2. Left: error measured in L^2 norm. Right: error measured in H^2 norm.

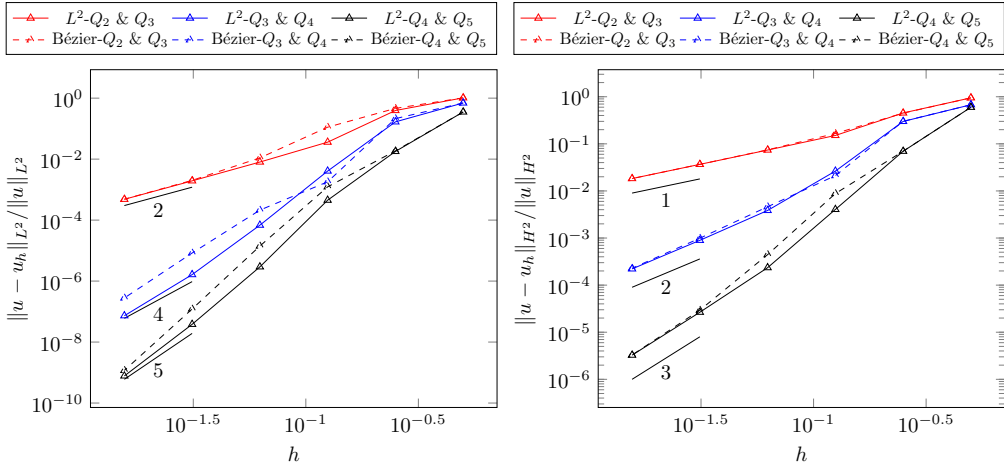


Figure 16: Convergence plot for degree mismatched non-conforming patch coupling in 7.2. Left: error measured in L^2 norm. Right: error measured in H^2 norm.

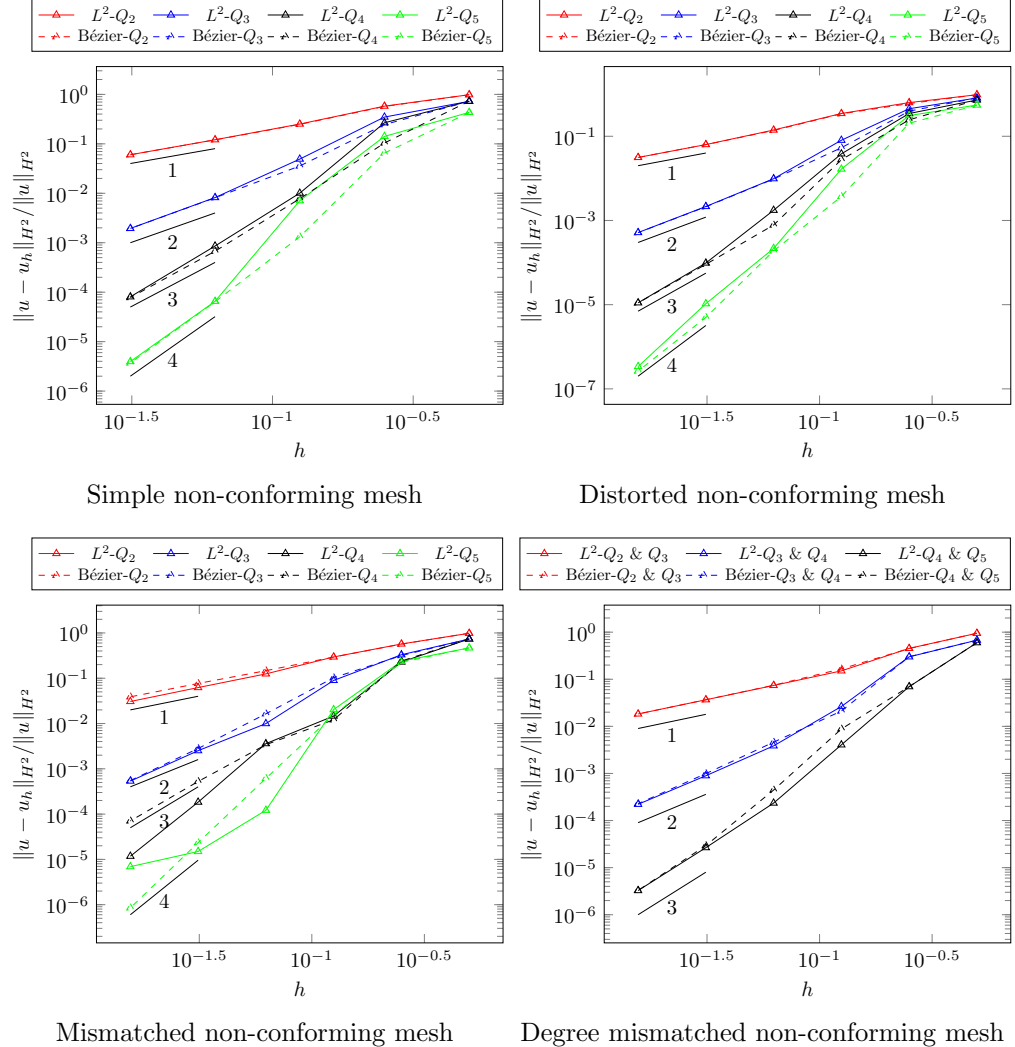
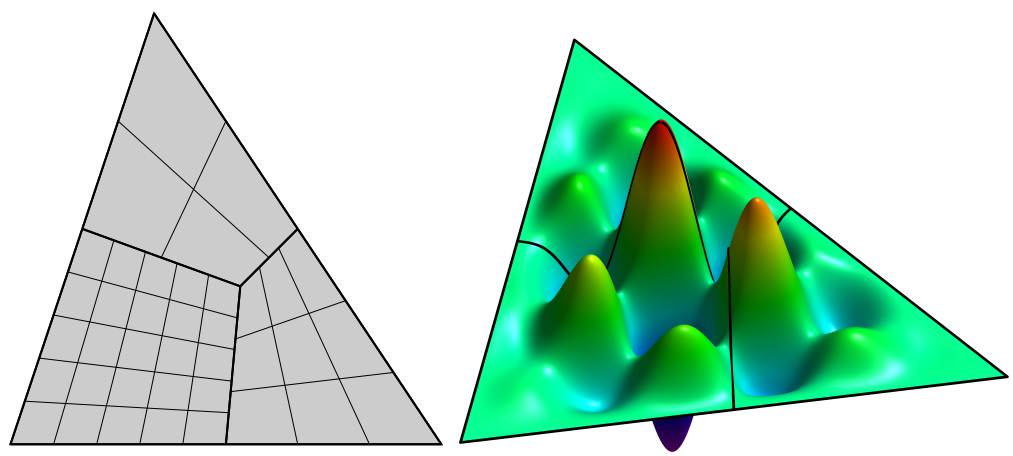


Figure 17: Convergence plot of the best H^2 approximation error for non-conforming patch coupling in 7.2.



(a) Non-conforming mesh

(b) Reference solution

Figure 18: The three-patch domain parameterization and the manufactured solution for Section 7.3.

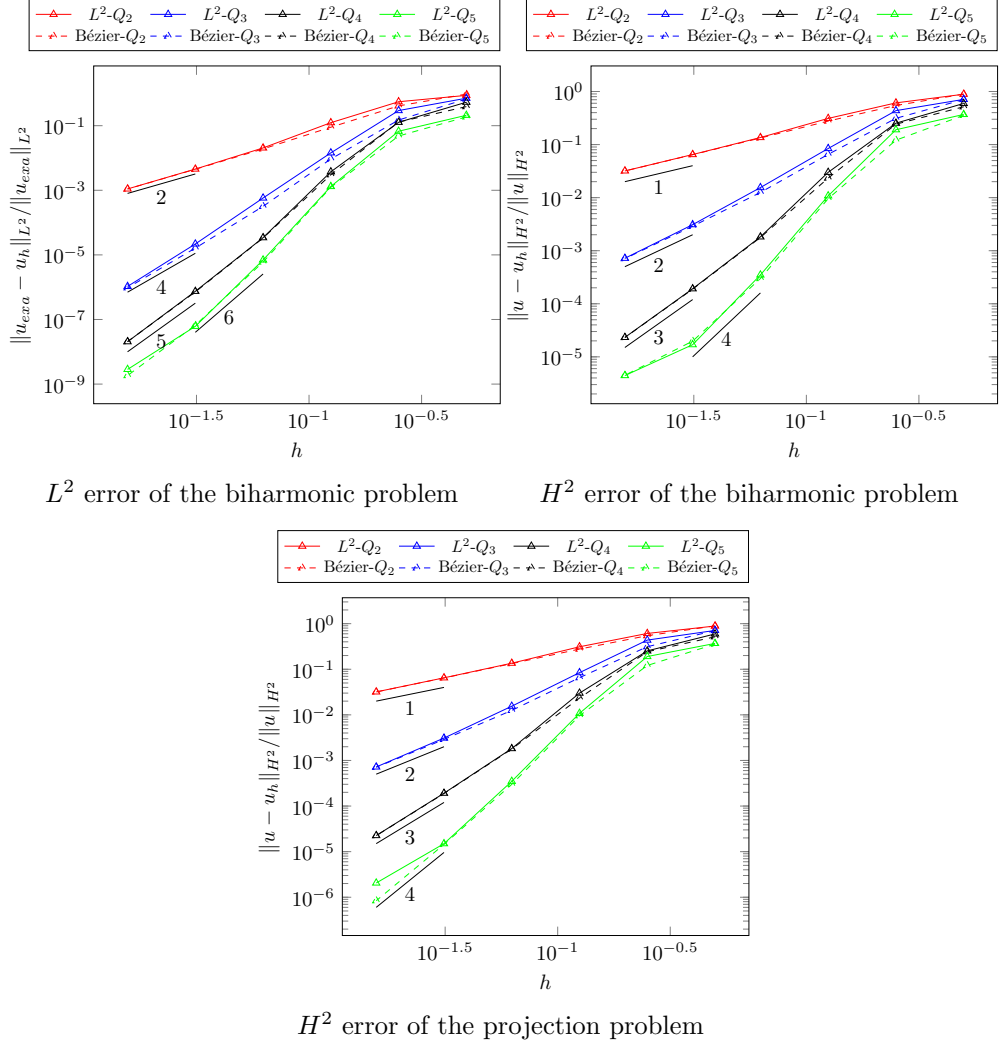


Figure 19: Convergence plots for the biharmonic problem on the three-patch domain in Section 7.3.

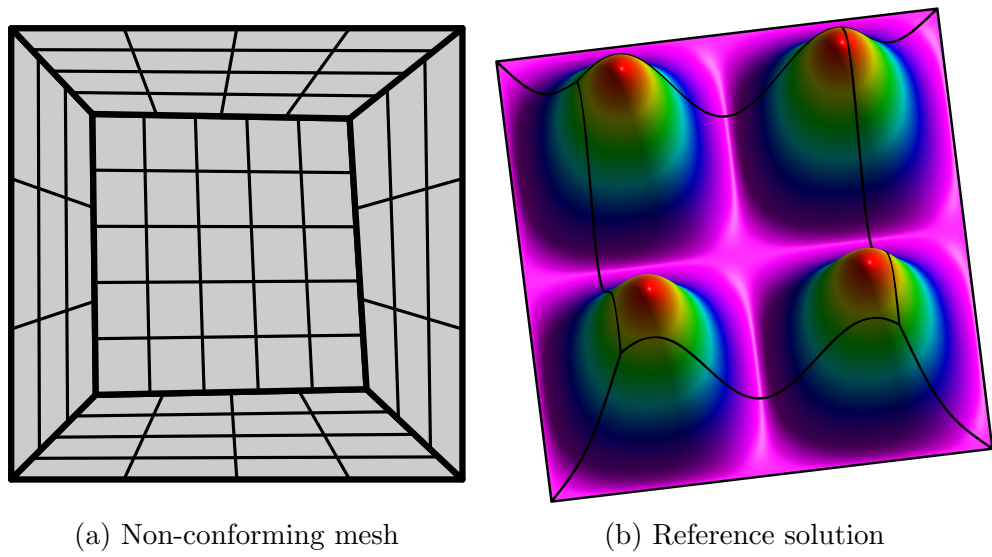


Figure 20: The three-patch domain parameterization and the manufactured solution for Section 7.3.

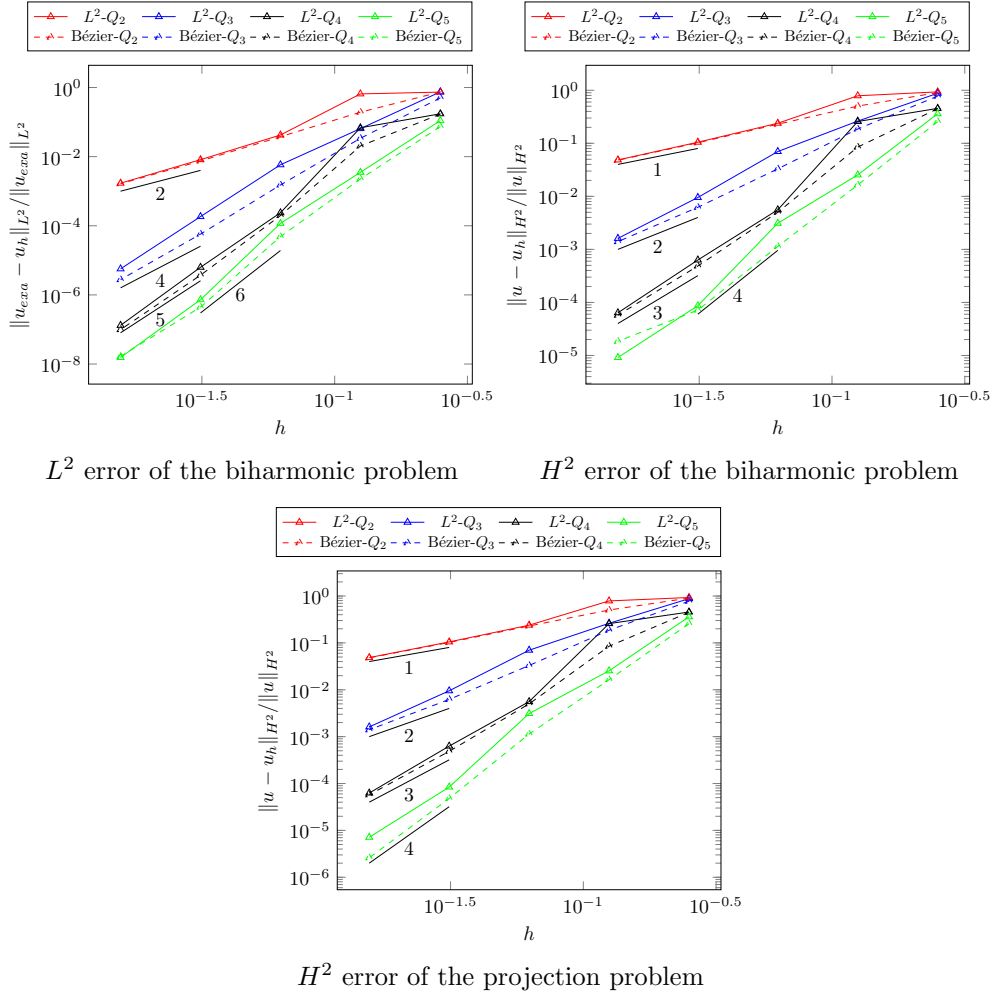
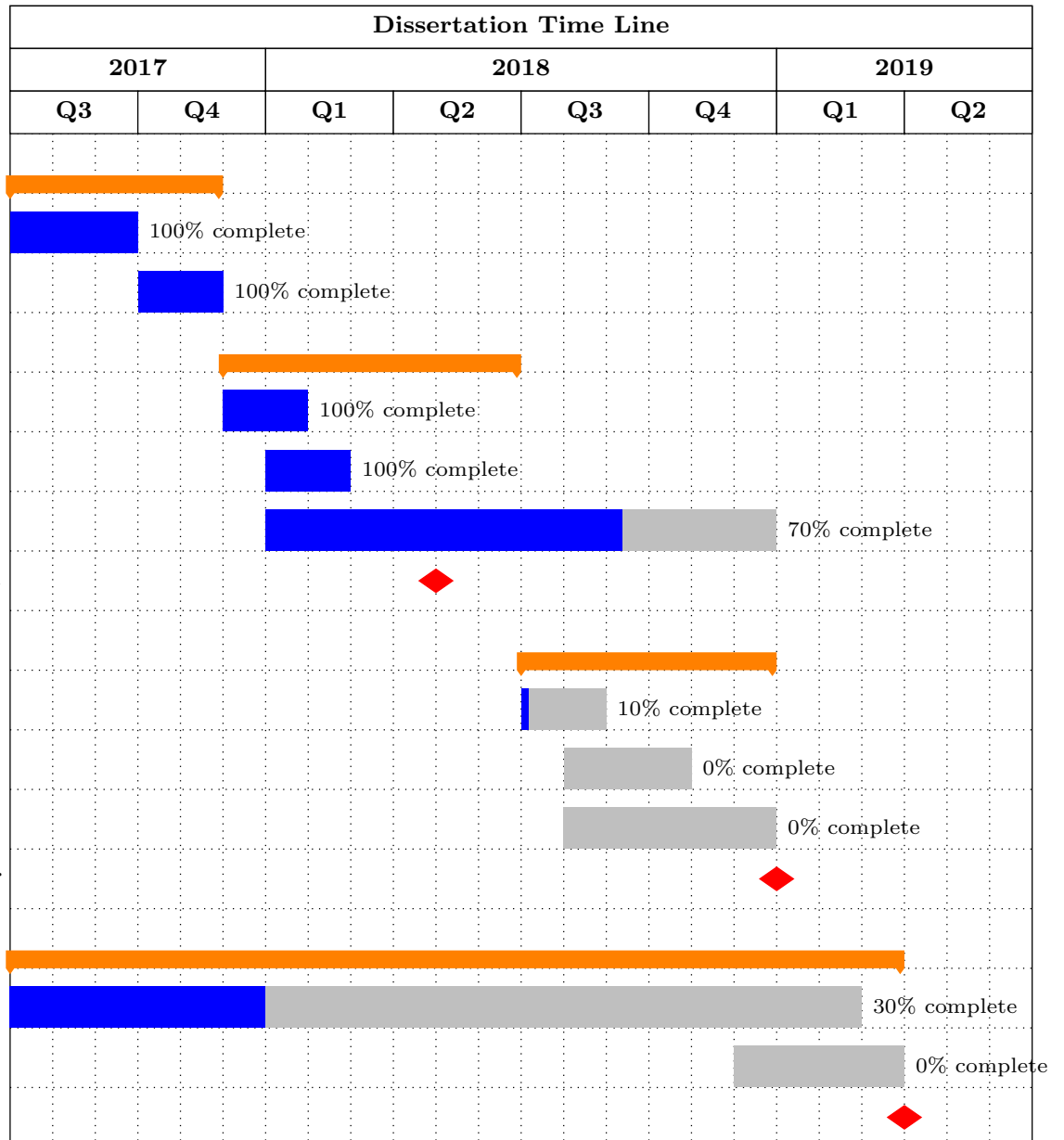
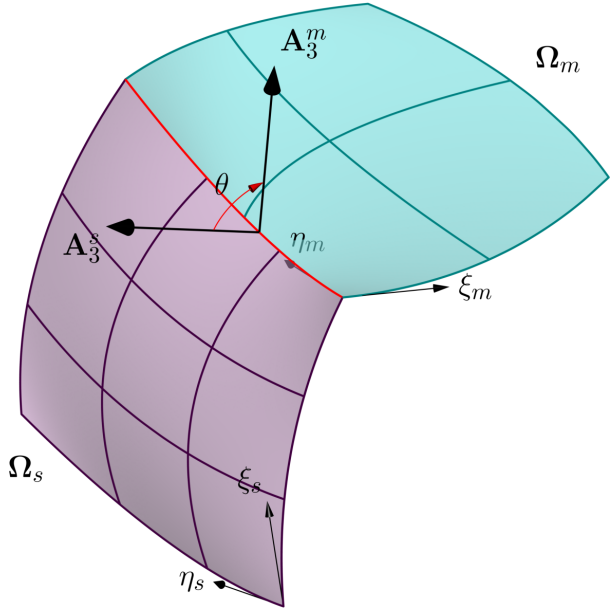


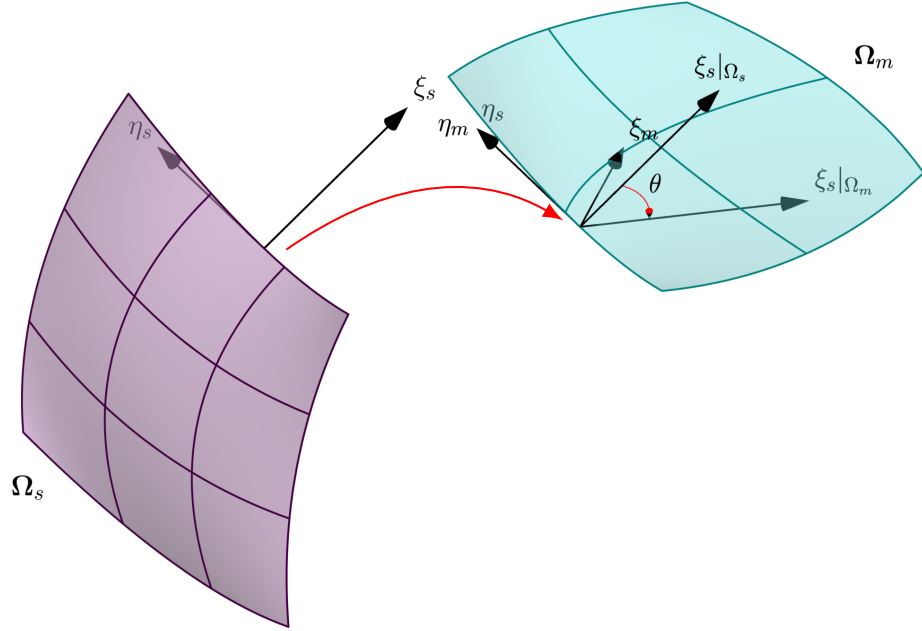
Figure 21: Convergence plots for the biharmonic problem on the five-patch domain in Section 7.3.

Table 2: A schedule of tasks and stages of my research towards the final dissertation.



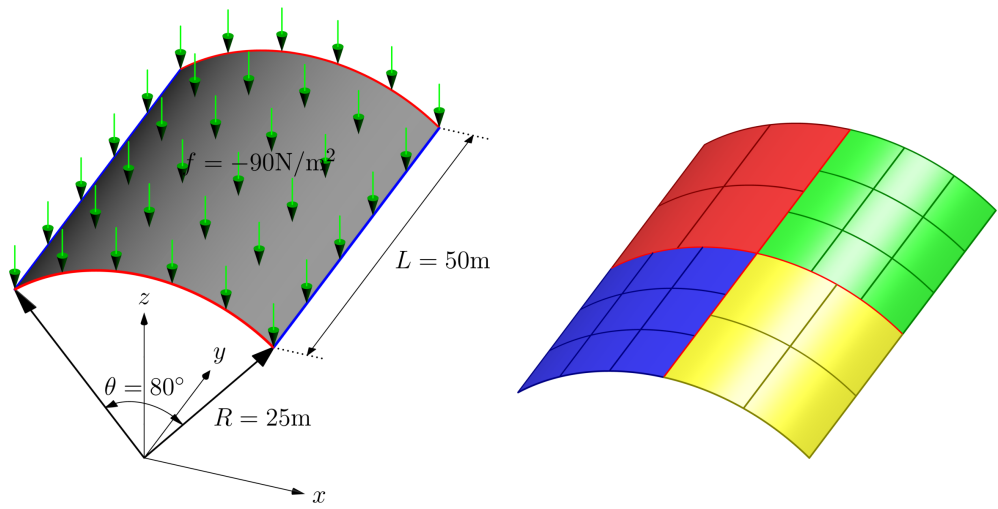


(a) A two patch non-conforming Kirchhoff-Love shell with the intersection denoted by the red line. The directors on each side of the intersection determine a rotation angle θ .



(b) The local coordinate system on the slave patch Ω_s is rotated and mapped to the master patch Ω_m .

Figure 22: A two patch non-conforming Kirchhoff-Love shell configuration illustrating the coupling with the appearance of kinks.



(a) Structure and boundary conditions for the problem. The blue edges are free, while (b) Non-conforming four patch mesh with the red edges are fixed in x and z directions. the intersections denoted by red lines.

Figure 23: The structure and mesh setup of the Scordelis-Lo roof problem.

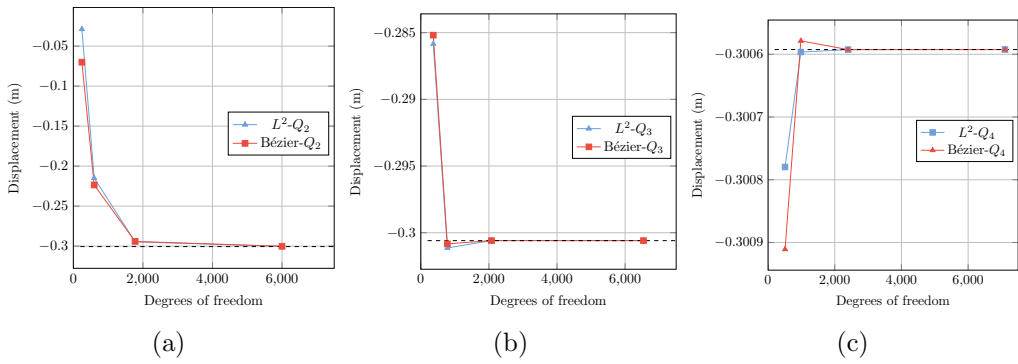


Figure 24: Scordelis-Lo roof: comparison of the vertical displacement at the midpoint of the free edge for different methods and degrees.



Figure 25: Deformed Scordelis-Lo roof (scaling factor of 20 is applied to the displacement):
(a) Only the C^0 continuity constraint is applied. Kinks are obvious for all intersections.
(b) The C^1 continuity constraint is also applied. The deformed surface is as smooth as a single patch.

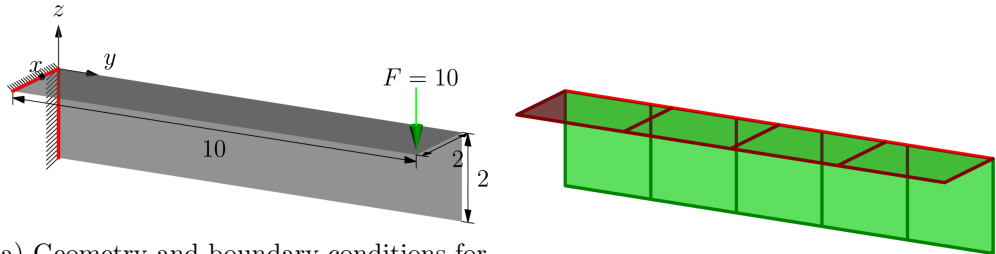


Figure 26: The geometry and mesh setup of the L-shaped cantilever beam problem.

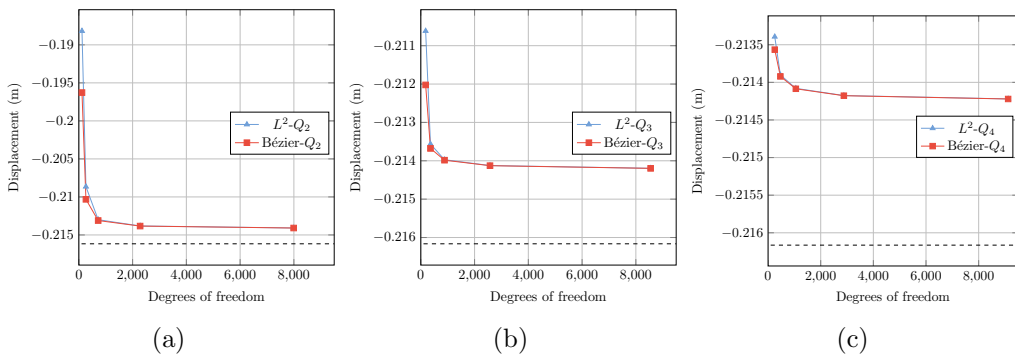


Figure 27: Scordelis-Lo roof: comparison of the vertical displacement at the loaded tip for different methods and degrees.

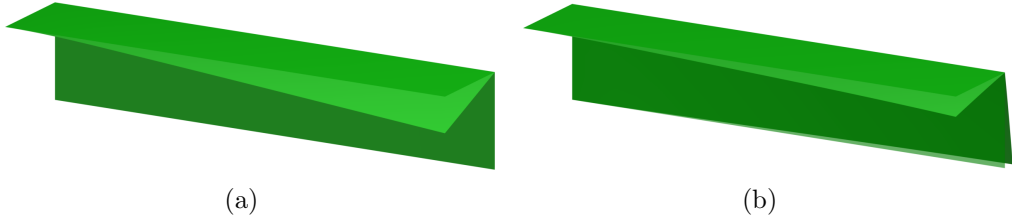
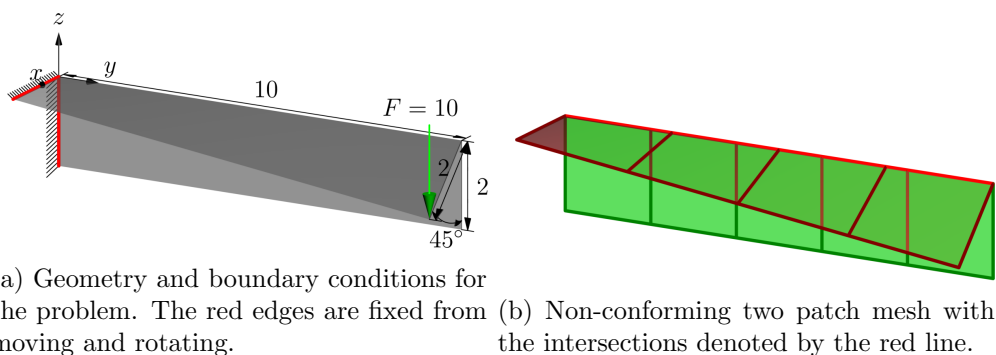


Figure 28: Deformed L-shaped cantilever beam (scaling factor of 10 is applied to the displacement): (a) Only the C^0 continuity constraint is applied. The kink serves like a hinge. (b) The proposed continuity constraint is also applied. The 90° angle between two patches is preserved.



(a) Geometry and boundary conditions for the problem. The red edges are fixed from moving and rotating. (b) Non-conforming two patch mesh with the intersections denoted by the red line.

Figure 29: The geometry and mesh setup of the L-shaped cantilever beam with variant angles.

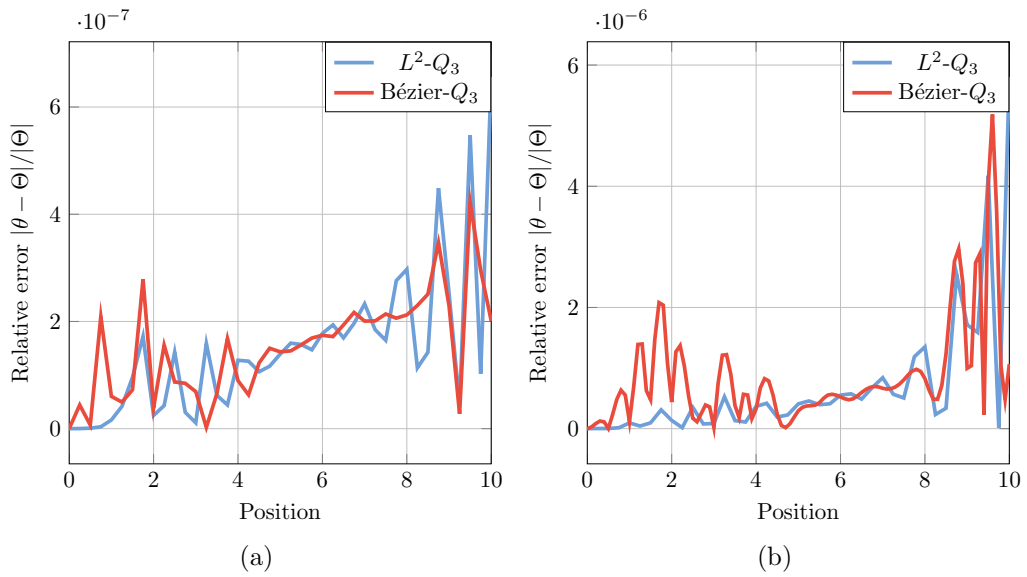


Figure 30: Relative errors of the deformed coupling angle for : (a) The L-shaped beam with a constant coupling angle of 90° . (b) The L-shaped beam with variant coupling angles.

- 956 [1] Andreas Apostolatos, Michael Breitenberger, Roland Wüchner, and Kai-
 957 Uwe Bletzinger. Domain decomposition methods and kirchhoff-love shell
 958 multipatch coupling in isogeometric analysis. In *Isogeometric Analysis*
 959 and Applications 2014, pages 73–101. Springer, 2015.
- 960 [2] Andreas Apostolatos, Robert Schmidt, Roland Wüchner, and Kai-Uwe
 961 Bletzinger. A Nitsche-type formulation and comparison of the most
 962 common domain decomposition methods in isogeometric analysis. *International*
 963 *Journal for Numerical Methods in Engineering*, 97(7):473–504,
 964 February 2014.
- 965 [3] Helio JC Barbosa and Thomas JR Hughes. The finite element method
 966 with lagrange multipliers on the boundary: circumventing the babuška-
 967 brezzi condition. *Computer Methods in Applied Mechanics and Engi-*
 968 *neering*, 85(1):109–128, 1991.
- 969 [4] Y. Bazilevs, V. M. Calo, J. A. Cottrell, J. A. Evans, T. J. R. Hughes,
 970 S. Lipton, M. A. Scott, and T. W. Sederberg. Isogeometric analysis using
 971 T-splines. *Computer Methods in Applied Mechanics and Engineering*,
 972 199(5–8):229–263, January 2010.
- 973 [5] Yuri Bazilevs, L Beirao da Veiga, J Austin Cottrell, Thomas JR Hughes,
 974 and Giancarlo Sangalli. Isogeometric analysis: approximation, stabil-
 975 ity and error estimates for h-refined meshes. *Mathematical Models and*
 976 *Methods in Applied Sciences*, 16(07):1031–1090, 2006.
- 977 [6] Roland Becker, Peter Hansbo, and Rolf Stenberg. A finite ele-
 978 ment method for domain decomposition with non-matching grids.
 979 *ESAIM: Mathematical Modelling and Numerical Analysis - Modélisation*
 980 *Mathématique et Analyse Numérique*, 37(2):209–225, 2003.
- 981 [7] F. B. Belgacem, P. Hild, and P. Laborde. The mortar finite element
 982 method for contact problems. *Mathematical and Computer Modelling*,
 983 28(4):263–271, August 1998.
- 984 [8] Faker Ben Belgacem. The Mortar finite element method with Lagrange
 985 multipliers. *Numerische Mathematik*, 84(2):173–197, December 1999.
- 986 [9] FAKER BEN BELGACEM, Patrick Hild, and Patrick Laborde. Ex-
 987 tension of the mortar finite element method to a variational inequality

- 988 modeling unilateral contact. *Mathematical Models and Methods in Applied Sciences*, 9(02):287–303, 1999.
- 990 [10] Zakaria Belhachmi and Christine Bernardi. Resolution of fourth-order
991 problems by the mortar element method. *Computer Methods in Applied Mechanics and Engineering*, 116(1):53–58, January 1994.
- 993 [11] Michele Benzi and Andrew J. Wathen. Some Preconditioning Techniques for Saddle Point Problems. In Wilhelmus H. A. Schilders, Henk A. van der Vorst, and Joost Rommes, editors, *Model Order Reduction: Theory, Research Aspects and Applications*, number 13 in Mathematics in Industry, pages 195–211. Springer Berlin Heidelberg, 2008. DOI: 10.1007/978-3-540-78841-6_10.
- 999 [12] Michel Bercovier and Tanya Matskewich. Smooth Bezier Surfaces over Arbitrary Quadrilateral Meshes. *arXiv:1412.1125 [math]*, December 1000 2014. arXiv: 1412.1125.
- 1002 [13] C. Bernardi, Y. Maday, and A. T. Patera. Domain Decomposition by 1003 the Mortar Element Method. In Hans G. Kaper, Marc Garbey, and 1004 Gail W. Pieper, editors, *Asymptotic and Numerical Methods for Partial 1005 Differential Equations with Critical Parameters*, pages 269–286. Springer 1006 Netherlands, Dordrecht, 1993. DOI: 10.1007/978-94-011-1810-1_17.
- 1007 [14] Christine Bernardi, Yvon Maday, and Francesca Rapetti. Basics and 1008 some applications of the mortar element method. *GAMM-Mitteilungen*, 1009 28(2):97–123, November 2005.
- 1010 [15] Manfred Bischoff, E Ramm, and J Irslinger. Models and finite elements 1011 for thin-walled structures. *Encyclopedia of Computational Mechanics* 1012 *Second Edition*, pages 1–86, 2018.
- 1013 [16] Daniele Boffi, Franco Brezzi, and Michel Fortin. *Mixed Finite Element 1014 Methods and Applications*. Springer Series in Computational Mathematics 1015 Springer-Verlag.
- 1016 [17] Michael J Borden, Thomas JR Hughes, Chad M Landis, and Clemens V 1017 Verhoosel. A higher-order phase-field model for brittle fracture: Formulation 1018 and analysis within the isogeometric analysis framework. *Computer Methods in 1019 Applied Mechanics and Engineering*, 273:100–118, 2014.
- 1020

- 1021 [18] Michael J Borden, Clemens V Verhoosel, Michael A Scott, Thomas JR
 1022 Hughes, and Chad M Landis. A phase-field description of dynamic brit-
 1023 tle fracture. *Computer Methods in Applied Mechanics and Engineering*,
 1024 217:77–95, 2012.
- 1025 [19] P. B. Bornemann and F. Cirak. A subdivision-based implementation of
 1026 the hierarchical b-spline finite element method. *Computer Methods in*
 1027 *Applied Mechanics and Engineering*, 253:584–598, January 2013.
- 1028 [20] Robin Bouclier, Jean-Charles Passieux, and Michel Salaün. Develop-
 1029 ment of a new, more regular, mortar method for the coupling of NURBS
 1030 subdomains within a NURBS patch: Application to a non-intrusive local
 1031 enrichment of NURBS patches. *Computer Methods in Applied Mechan-
 1032 ics and Engineering*, 316:123–150, April 2017.
- 1033 [21] Susanne Brenner and Ridgway Scott. *The Mathematical Theory of Fi-
 1034 nite Element Methods*. Springer Science & Business Media, December
 1035 2007. Google-Books-ID: ci4c_R0WKYYC.
- 1036 [22] Ericka Brivadis, Annalisa Buffa, Barbara Wohlmuth, and Linus Wun-
 1037 derlich. Isogeometric mortar methods. *Computer Methods in Applied
 1038 Mechanics and Engineering*, 284:292–319, February 2015.
- 1039 [23] A. Buffa, D. Cho, and G. Sangalli. Linear independence of the T-spline
 1040 blending functions associated with some particular T-meshes. *Computer
 1041 Methods in Applied Mechanics and Engineering*, 199(23–24):1437–1445,
 1042 April 2010.
- 1043 [24] E. Catmull and J. Clark. Recursively generated B-spline surfaces on
 1044 arbitrary topological meshes. *Computer-Aided Design*, 10(6):350–355,
 1045 November 1978.
- 1046 [25] Franz Chouly, Patrick Hild, and Yves Renard. Symmetric and non-
 1047 symmetric variants of Nitsche’s method for contact problems in elasticity:
 1048 theory and numerical experiments. *Mathematics of Computation*,
 1049 84(293):1089–1112, 2015.
- 1050 [26] Annabelle Collin, Giancarlo Sangalli, and Thomas Takacs. Analysis-
 1051 suitable G1 multi-patch parametrizations for C1 isogeometric spaces.
 1052 *Computer Aided Geometric Design*, 47:93–113, October 2016.

- 1053 [27] Laurens Coox, Onur Atak, Dirk Vandepitte, and Wim Desmet. An isogeometric
 1054 indirect boundary element method for solving acoustic problems
 1055 in open-boundary domains. *Computer Methods in Applied Mechanics and Engineering*, 316:186–208, April 2017.
- 1057 [28] Laurens Coox, Francesco Greco, Onur Atak, Dirk Vandepitte, and Wim
 1058 Desmet. A robust patch coupling method for NURBS-based isogeometric
 1059 analysis of non-conforming multipatch surfaces. *Computer Methods in Applied Mechanics and Engineering*, 316:235–260, April 2017.
- 1061 [29] Laurens Coox, Florian Maurin, Francesco Greco, Elke Deckers, Dirk
 1062 Vandepitte, and Wim Desmet. A flexible approach for coupling nurbs
 1063 patches in rotationless isogeometric analysis of kirchhoff–love shells.
 1064 *Computer Methods in Applied Mechanics and Engineering*, 325:505–531,
 1065 2017.
- 1066 [30] L Beirao Da Veiga, Annalisa Buffa, Judith Rivas, and Giancarlo Sangalli.
 1067 Some estimates for h–p–k-refinement in isogeometric analysis. *Numerische Mathematik*, 118(2):271–305, 2011.
- 1069 [31] L Beirao Da Veiga, Annalisa Buffa, Giancarlo Sangalli, and Rafael
 1070 Vázquez. Mathematical analysis of variational isogeometric methods.
 1071 *Acta Numerica*, 23:157–287, 2014.
- 1072 [32] D. Doo and M. Sabin. Behaviour of recursive division surfaces near ex-
 1073 traordinary points. *Computer-Aided Design*, 10(6):356–360, November
 1074 1978.
- 1075 [33] W Dornisch, J Stöckler, and R Müller. Dual and approximate dual
 1076 basis functions for b-splines and nurbs–comparison and application for
 1077 an efficient coupling of patches with the isogeometric mortar method.
 1078 *Computer Methods in Applied Mechanics and Engineering*, 316:449–496,
 1079 2017.
- 1080 [34] W. Dornisch, J. Stöckler, and R. Müller. Dual and approximate dual
 1081 basis functions for B-splines and NURBS – Comparison and application
 1082 for an efficient coupling of patches with the isogeometric mortar method.
 1083 *Computer Methods in Applied Mechanics and Engineering*, 316:449–496,
 1084 April 2017.

- 1085 [35] W. Dornisch, G. Vitucci, and S. Klinkel. The weak substitution method
 1086 – an application of the mortar method for patch coupling in NURBS-
 1087 based isogeometric analysis. *International Journal for Numerical Methods in Engineering*, 103(3):205–234, July 2015.
- 1089 [36] Wolfgang Dornisch and Sven Klinkel. Boundary conditions and multi-
 1090 patch connections in isogeometric analysis. *PAMM*, 11(1):207–208, 2011.
- 1091 [37] Wolfgang Dornisch and Ralf Müller. Patch coupling with the isogeomet-
 1092 ric dual mortar approach. *PAMM*, 16(1):193–194, October 2016.
- 1093 [38] Michael R. Dörfel, Bert Jüttler, and Bernd Simeon. Adaptive isogeomet-
 1094 ric analysis by local h-refinement with T-splines. *Computer Methods in*
 1095 *Applied Mechanics and Engineering*, 199(5–8):264–275, January 2010.
- 1096 [39] Anand Embar, John Dolbow, and Isaac Harari. Imposing Dirichlet
 1097 boundary conditions with Nitsche’s method and spline-based finite el-
 1098 ements. *International Journal for Numerical Methods in Engineering*,
 1099 83(7):877–898, August 2010.
- 1100 [40] Charbel Farhat, Po-Shu Chen, and Jan Mandel. A scalable Lagrange
 1101 multiplier based domain decomposition method for time-dependent
 1102 problems. *International Journal for Numerical Methods in Engineering*,
 1103 38(22):3831–3853, November 1995.
- 1104 [41] David R. Forsey and Richard H. Bartels. Hierarchical B-spline Re-
 1105 finement. In *Proceedings of the 15th Annual Conference on Computer*
 1106 *Graphics and Interactive Techniques*, SIGGRAPH ’88, pages 205–212,
 1107 New York, NY, USA, 1988. ACM.
- 1108 [42] Carlotta Giannelli, Bert Jüttler, and Hendrik Speleers. THB-splines:
 1109 The truncated basis for hierarchical splines. *Computer Aided Geometric*
 1110 *Design*, 29(7):485–498, October 2012.
- 1111 [43] Héctor Gómez, Victor M Calo, Yuri Bazilevs, and Thomas JR Hughes.
 1112 Isogeometric analysis of the cahn–hilliard phase-field model. *Computer*
 1113 *methods in applied mechanics and engineering*, 197(49-50):4333–4352,
 1114 2008.

- 1115 [44] David Girois and Jörg Peters. Matched -constructions always yield
 1116 -continuous isogeometric elements. *Computer Aided Geometric Design*,
 1117 34:67–72, March 2015.
- 1118 [45] Yujie Guo and Martin Ruess. Nitsche’s method for a coupling of isoge-
 1119 ometric thin shells and blended shell structures. *Computer Methods in*
 1120 *Applied Mechanics and Engineering*, 284:881–905, February 2015.
- 1121 [46] Peter Hansbo. Nitsche’s method for interface problems in computa-
 1122 tional mechanics. *GAMM-Mitteilungen*, 28(2):183–206, November 2005.
- 1123 [47] Peter Hansbo, Carlo Lovadina, Ilaria Perugia, and Giancarlo Sangalli. A
 1124 lagrange multiplier method for the finite element solution of elliptic in-
 1125 terface problems using non-matching meshes. *Numerische Mathematik*,
 1126 100(1):91–115, 2005.
- 1127 [48] Christian Hesch and Peter Betsch. Isogeometric analysis and domain
 1128 decomposition methods. *Computer Methods in Applied Mechanics and*
 1129 *Engineering*, 213–216:104–112, March 2012.
- 1130 [49] Stefan Hüeber and Barbara I Wohlmuth. A primal–dual active set strat-
 1131 egy for non-linear multibody contact problems. *Computer Methods in*
 1132 *Applied Mechanics and Engineering*, 194(27-29):3147–3166, 2005.
- 1133 [50] T.J.R. Hughes, J.A. Cottrell, and Y. Bazilevs. Isogeometric analysis:
 1134 Cad, finite elements, nurbs, exact geometry and mesh refinement. *Com-*
 1135 *puter Methods in Applied Mechanics and Engineering*, 194(39):4135 –
 1136 4195, 2005.
- 1137 [51] Mika Juntunen. On the connection between the stabilized lagrange mul-
 1138 tiplier and nitsche’s methods. *Numerische Mathematik*, 131(3):453–471,
 1139 2015.
- 1140 [52] Bert Jüttler, Angelos Mantzaflaris, Ricardo Perl, and Martin Rumpf.
 1141 On numerical integration in isogeometric subdivision methods for PDEs
 1142 on surfaces. *Computer Methods in Applied Mechanics and Engineering*,
 1143 302:131–146, April 2016.
- 1144 [53] Hongmei Kang, Xin Li, Falai Chen, and Jiansong Deng. Truncated
 1145 Hierarchical Loop Subdivision Surfaces and application in isogeometric

- 1146 analysis. *Computers & Mathematics with Applications*, 72(8):2041–2055,
 1147 October 2016.
- 1148 [54] Mario Kapl, Florian Buchegger, Michel Bercovier, and Bert Jüttler. Iso-
 1149 geometric analysis with geometrically continuous functions on planar
 1150 multi-patch geometries. *Computer Methods in Applied Mechanics and*
 1151 *Engineering*, 316:209–234, April 2017.
- 1152 [55] Mario Kapl and Vito Vitrih. Space of -smooth geometrically continuous
 1153 isogeometric functions on planar multi-patch geometries: Dimension and
 1154 numerical experiments. *Computers & Mathematics with Applications*.
- 1155 [56] Mario Kapl and Vito Vitrih. Space of -smooth geometrically continuous
 1156 isogeometric functions on two-patch geometries. *Computers & Mathe-*
 1157 *matics with Applications*, 73(1):37–59, January 2017.
- 1158 [57] Mario Kapl, Vito Vitrih, Bert Jüttler, and Katharina Birner. Isoge-
 1159 ometric analysis with geometrically continuous functions on two-patch
 1160 geometries. *Computers & Mathematics with Applications*, 70(7):1518–
 1161 1538, October 2015.
- 1162 [58] J Kiendl, Y Bazilevs, M-C Hsu, R Wüchner, and K-U Bletzinger. The
 1163 bending strip method for isogeometric analysis of kirchhoff–love shell
 1164 structures comprised of multiple patches. *Computer Methods in Applied*
 1165 *Mechanics and Engineering*, 199(37-40):2403–2416, 2010.
- 1166 [59] J Kiendl, K-U Bletzinger, J Linhard, and R Wüchner. Isogeometric shell
 1167 analysis with kirchhoff–love elements. *Computer Methods in Applied*
 1168 *Mechanics and Engineering*, 198(49-52):3902–3914, 2009.
- 1169 [60] Josef Kiendl, Ming-Chen Hsu, Michael CH Wu, and Alessandro Reali.
 1170 Isogeometric kirchhoff–love shell formulations for general hyperelastic
 1171 materials. *Computer Methods in Applied Mechanics and Engineering*,
 1172 291:280–303, 2015.
- 1173 [61] Bishnu Prasad Lamichhane. Higher order mortar finite elements with
 1174 dual lagrange multiplier spaces and applications.
- 1175 [62] Bishnu Prasad Lamichhane and Barbara I Wohlmuth. Higher order
 1176 dual lagrange multiplier spaces for mortar finite element discretizations.
 1177 *Calcolo*, 39(4):219–237, 2002.

- 1178 [63] Xin Li and M. A. Scott. Analysis-suitable T-splines: Characterization,
 1179 refineability, and approximation. *Mathematical Models and Methods in*
 1180 *Applied Sciences*, 24(06):1141–1164, October 2013.
- 1181 [64] Xin Li, Jianmin Zheng, Thomas W. Sederberg, Thomas J. R. Hughes,
 1182 and Michael A. Scott. On linear independence of T-spline blending func-
 1183 tions. *Computer Aided Geometric Design*, 29(1):63–76, January 2012.
- 1184 [65] Charles Teorell Loop and Charles Loop. Smooth Subdivision Surfaces
 1185 Based on Triangles. January 1987.
- 1186 [66] Leszek Marcinkowski. Mortar methods for some second and fourth order
 1187 elliptic equations. *Distinguished Ph. D. Thesis*, 1999.
- 1188 [67] Stephen E Moore. Discontinuous galerkin isogeometric analysis for the
 1189 biharmonic equation. *arXiv preprint arXiv:1703.02726*, 2017.
- 1190 [68] Thien Nguyen, Keçstutis Karčiauskas, and Jörg Peters. A Comparative
 1191 Study of Several Classical, Discrete Differential and Isogeometric Meth-
 1192 ods for Solving Poisson’s Equation on the Disk. *Axioms*, 3(2):280–299,
 1193 June 2014.
- 1194 [69] Vinh Phu Nguyen, Pierre Kerfriden, Marco Brino, Stéphane P. A. Bor-
 1195 das, and Elvio Bonisoli. Nitsche’s method for two and three dimensional
 1196 NURBS patch coupling. *Computational Mechanics*, 53(6):1163–1182,
 1197 June 2014.
- 1198 [70] J. Nitsche. Über ein Variationsprinzip zur Lösung von Dirichlet-
 1199 Problemen bei Verwendung von Teilräumen, die keinen Randbedingun-
 1200 gen unterworfen sind. *Abhandlungen aus dem Mathematischen Seminar
 1201 der Universität Hamburg*, 36(1):9–15, July 1971.
- 1202 [71] Peter Oswald and Barbara Wohlmuth. On polynomial reproduction of
 1203 dual fe bases. In *Thirteenth international conference on domain decom-
 1204 position methods*, pages 85–96, 2001.
- 1205 [72] Qing Pan, Guoliang Xu, Gang Xu, and Yongjie Zhang. Isogeometric
 1206 analysis based on extended Loop’s subdivision. *Journal of Compu-
 1207 tational Physics*, 299:731–746, October 2015.

- 1208 [73] Jörg Peters. Joining smooth patches around a vertex to form a C_k
 1209 surface. *Computer Aided Geometric Design*, 9(5):387–411, November
 1210 1992.
- 1211 [74] Jörg Peters. Chapter 8 - Geometric Continuity. In *Handbook of Com-*
 1212 *puter Aided Geometric Design*, pages 193–227. North-Holland, Amster-
 1213 dam, 2002. DOI: 10.1016/B978-044451104-1/50009-5.
- 1214 [75] Alexander Popp, Michael W Gee, and Wolfgang A Wall. A finite de-
 1215 formation mortar contact formulation using a primal–dual active set
 1216 strategy. *International Journal for Numerical Methods in Engineering*,
 1217 79(11):1354–1391, 2009.
- 1218 [76] Beatrice Riviere. *Discontinuous Galerkin methods for solving elliptic*
 1219 *and parabolic equations: theory and implementation*. SIAM, 2008.
- 1220 [77] AC Scordelis and KS Lo. Computer analysis of cylindrical shells. In
 1221 *Journal Proceedings*, volume 61, pages 539–562, 1964.
- 1222 [78] M. A. Scott, X. Li, T. W. Sederberg, and T. J. R. Hughes. Local
 1223 refinement of analysis-suitable T-splines. *Computer Methods in Applied*
 1224 *Mechanics and Engineering*, 213–216:206–222, March 2012.
- 1225 [79] M. A. Scott, R. N. Simpson, J. A. Evans, S. Lipton, S. P. A. Bordas,
 1226 T. J. R. Hughes, and T. W. Sederberg. Isogeometric boundary element
 1227 analysis using unstructured T-splines. *Computer Methods in Applied*
 1228 *Mechanics and Engineering*, 254:197–221, February 2013.
- 1229 [80] Michael A. Scott, Michael J. Borden, Clemens V. Verhoosel, Thomas W.
 1230 Sederberg, and Thomas J. R. Hughes. Isogeometric finite element data
 1231 structures based on Bézier extraction of T-splines. *International Journal*
 1232 *for Numerical Methods in Engineering*, 88(2):126–156, October 2011.
- 1233 [81] Thomas W. Sederberg, Jianmin Zheng, Almaz Bakenov, and Ahmad
 1234 Nasri. T-splines and T-NURCCs. In *ACM SIGGRAPH 2003 Papers*,
 1235 SIGGRAPH ’03, pages 477–484, New York, NY, USA, 2003. ACM.
- 1236 [82] Alexander Seitz, Philipp Farah, Johannes Kremheller, Barbara I.
 1237 Wohlmuth, Wolfgang A. Wall, and Alexander Popp. Isogeometric dual
 1238 mortar methods for computational contact mechanics. *Computer Meth-*
 1239 *ods in Applied Mechanics and Engineering*, 301:259–280, April 2016.

- 1240 [83] Juan C Simo, Peter Wriggers, and Robert L Taylor. A perturbed la-
 1241 grangian formulation for the finite element solution of contact problems.
 1242 *Computer methods in applied mechanics and engineering*, 50(2):163–180,
 1243 1985.
- 1244 [84] Rolf Stenberg. On some techniques for approximating boundary con-
 1245 ditions in the finite element method. *Journal of Computational and*
 1246 *applied Mathematics*, 63(1-3):139–148, 1995.
- 1247 [85] Gilbert Strang and George Fix. *An Analysis of the Finite Element*
 1248 *Method*. Wellesley-Cambridge Press, May 2008. Google-Books-ID:
 1249 K5MAOwAACAAJ.
- 1250 [86] Radek Tezaur. *Analysis of Lagrange multiplier based domain decompo-*
 1251 *sition*. PhD thesis, University of Colorado at Denver, 1998.
- 1252 [87] Derek C Thomas, Michael A Scott, John A Evans, Kevin Tew, and
 1253 Emily J Evans. Bézier projection: a unified approach for local pro-
 1254 jection and quadrature-free refinement and coarsening of nurbs and t-
 1255 splines with particular application to isogeometric design and analysis.
 1256 *Computer Methods in Applied Mechanics and Engineering*, 284:55–105,
 1257 2015.
- 1258 [88] Manuel Tur, Jose Albelda, Jose Manuel Navarro-Jimenez, and Juan Jose
 1259 Rodenas. A modified perturbed lagrangian formulation for contact prob-
 1260 lems. *Computational Mechanics*, 55(4):737–754, 2015.
- 1261 [89] A. V. Vuong, C. Giannelli, B. Jüttler, and B. Simeon. A hierarchical ap-
 1262 proach to adaptive local refinement in isogeometric analysis. *Computer*
 1263 *Methods in Applied Mechanics and Engineering*, 200(49–52):3554–3567,
 1264 December 2011.
- 1265 [90] Xiaodong Wei, Yongjie Zhang, Thomas J. R. Hughes, and Michael A.
 1266 Scott. Truncated hierarchical Catmull–Clark subdivision with local re-
 1267 finement. *Computer Methods in Applied Mechanics and Engineering*,
 1268 291:1–20, July 2015.
- 1269 [91] B. Wohlmuth. A Mortar Finite Element Method Using Dual Spaces
 1270 for the Lagrange Multiplier. *SIAM Journal on Numerical Analysis*,
 1271 38(3):989–1012, January 2000.

- 1272 [92] Barbara I Wohlmuth. A comparison of dual lagrange multiplier spaces
1273 for mortar finite element discretizations. *ESAIM: Mathematical Mod-*
1274 *elling and Numerical Analysis*, 36(6):995–1012, 2002.
- 1275 [93] Xin Li. Some Properties for Analysis-Suitable T-Splines. *Journal of*
1276 *Computational Mathematics*, 33(4):428–442, July 2015.
- 1277 [94] Olgierd Cecil Zienkiewicz, Robert Leroy Taylor, Olgierd Cecil
1278 Zienkiewicz, and Robert Lee Taylor. *The finite element method*, vol-
1279 ume 3. McGraw-hill London, 1977.
- 1280 [95] Z Zou, MA Scott, MJ Borden, DC Thomas, W Dornisch, and E Brivadis.
1281 Isogeometric b  zier dual mortaring: Refineable higher-order spline dual
1282 bases and weakly continuous geometry. *Computer Methods in Applied*
1283 *Mechanics and Engineering*, 333:497–534, 2018.